

December 19, 2012

# Dark radiation from particle decay: cosmological constraints and opportunities

Jasper Hasenkamp and Jörn Kersten

*II. Institute for Theoretical Physics, University of Hamburg, 22761 Hamburg, Germany*

Jasper.Hasenkamp@desy.de, Joern.Kersten@desy.de

## Abstract

We study particle decay as the origin of dark radiation. After elaborating general properties and useful parametrisations we provide model-independent and easy-to-use constraints from nucleosynthesis, the cosmic microwave background and structure formation. Bounds on branching ratios and mass hierarchies depend in a unique way on the time of decay. We demonstrate their power to exclude well-motivated scenarios taking the example of the lightest ordinary sparticle decaying into the gravitino. We point out signatures and opportunities in cosmological observations and structure formation. For example, if there are two dark decay modes, dark radiation and the observed dark matter with adjustable free-streaming can originate from the same decay, solving small-scale problems of structure formation. Hot dark matter mimicking a neutrino mass scale as deduced from cosmological observations can arise and possibly be distinguished after a discovery. Our results can be used as a guideline for model building.

# 1 Introduction

New cosmological probes measure the amount of radiation in the Universe at different epochs of its evolution with a crucial increase in precision. One strength of the standard cosmological model, which is based upon general relativity and the Standard Model (SM) of particle physics amended by “invisible” components known as dark matter and dark energy, is the precise prediction of the amount of radiation. Within the first 20 minutes light nuclei like helium were formed during the process of big bang nucleosynthesis (BBN) as observed today. At such early times the Universe was dominated by radiation. Since nucleosynthesis depends on the expansion rate, BBN is sensitive to the amount of radiation. There is still a controversy between different groups, some favouring the prediction and others an increased amount [1, 2, 3]. Since the main uncertainty stems from the determination of the relic helium abundance from observations, we can expect improvements in the foreseeable future. Observations of the cosmic microwave background (CMB) constrain the amount of radiation in the Universe in an epoch lasting from some thousand years till photons decouple  $10^5$  years later. Since the first determination of the radiation content of the Universe from the CMB roughly ten years ago [4] and also in current measurements by the South Pole Telescope [5] and the Atacama Cosmology Telescope [6], mean values are larger than the prediction. The observed suppression of the CMB power spectrum at larger multipoles would be due to increased Silk damping [7]. Non-Gaussianities could provide further insights [8]. Additional radiation also eliminates tension between cosmological data and measurements of today’s expansion rate [9, 10]. Increased mean values are found as well in extended analyses including additional cosmological data [11, 12, 13, 14, 15, 16, 17, 18], although the results for the statistical significance of this increase vary. More importantly, due to the increase in precision [19, 20] the Planck satellite, which finished data taking already, could turn these hints into a  $3\text{-}\sigma$  to  $5\text{-}\sigma$  discovery, if current mean values are accurate. Our understanding of the third component in the Universe –besides matter and vacuum energy– would be proven incomplete, too. Since such additional, “invisible” radiation cannot arise from the SM and its nature is unknown, it has been dubbed dark radiation.

In this work we study particle decay as the origin of dark radiation. Additional radiation has been studied mainly in connection with the possible existence of additional neutrino species beyond the known three [21, 22, 23, 24] or other relativistic species [25, 26, 27]. The amount of additional radiation is then generically discrete. The species are relativistic during BBN and may or may not still be relativistic around photon decoupling. Hence, they always lead to an increase in radiation at BBN and generically the same increase during CMB times. This is an appealing prediction, in particular, because past observations have been too imprecise to find a difference between BBN and CMB determinations. In contrast, dark radiation from particle decay can originate before [28, 29, 30, 31, 32, 33], during or after BBN [34, 35, 36, 37, 38, 39, 40, 41] and can become non-relativistic before, during or after photon decoupling. Any observed value can be explained. These are qualitative differences to the case of a relativistic species that become distinguishable given the new observational precision. Even though current observations do not allow for any conclusion [7, 42], the most interesting finding would

be an increase in radiation after BBN. This would exclude additional relativistic species leaving late particle decay as the most attractive possibility.<sup>1</sup> Interestingly, the time of decay can be probed in the inflationary gravitational wave background [44].

We exploit the fact that the energy density of the decaying particle is fixed by the observed amount of dark radiation to determine model-independent upper bounds on several branching ratios of the decaying particle from BBN, spectral distortions in the CMB and the ionisation history of the Universe. Thereby, we point out an opportunity to solve the cosmological lithium problems [45] and the discovery potential of a future CMB polarimeter for the considered decay. A decay before BBN could mimic a cosmology with additional relativistic species. More importantly, there is a plethora of new cosmologies. We elaborate constraints and opportunities from heavier decay products in structure formation. They may just form dark radiation, but they do not need to act as radiation at all. If they form the observed dark matter, two of three dark components would originate from the same decay. If they are not cold, their free-streaming might resolve the missing satellites problem [46, 47]. While lighter decay products act as dark radiation, heavier ones might mimic the neutrino mass scale as deduced from cosmological observations. Cluster abundances seem to favour additional radiation together with a finite neutrino mass scale [48].

In the next section we study the simplest case allowing for exactly one dark decay mode. We will use our findings in Sec. 4 to explore which opportunities open up in structure formation, if there are two dark decay modes. Sec. 3 is devoted to general constraints and opportunities from BBN and CMB. We summarise and conclude in Sec. 5. In the appendix we provide an analytic treatment of the exponential decay law in an expanding universe.

## 2 One dark decay mode

In this section we study the origin of dark radiation from (one) two-body decay of a non-relativistic particle. Such a decay is drawn in the upper right corner of Fig. 1, where we indicate some nomenclature. The decaying particle (mother) decays into non-identical particles, where one is heavier (heavier daughter) and the other one lighter (lighter daughter). In Fig. 1 we illustrate the behaviour of certain energy densities in a cosmology with dark radiation from particle decay. First of all, the plethora of possible cosmologies cannot be shown in only one figure. So we illustrate a few typical and interesting scenarios. At some early time corresponding to a small scale factor the Universe is dominated by radiation and the mother is relativistic, so that their energy densities scale equally. At some time the mother becomes non-relativistic and from then on its energy density  $\rho \propto a^{-3}$  grows relative to the radiation energy density  $\rho_{\text{rad}} \propto a^{-4}$  as the Universe expands, where  $a$  denotes the growing scale factor. Thus stable or very long-lived matter generically comes to dominate the Universe. Actually, this fact gives rise to various cosmological problems with the well-known gravitino problem as prime example. These problems may turn out as fortunes, if they give rise to the desired

---

<sup>1</sup> One alternative is the late annihilation of additional species [43].

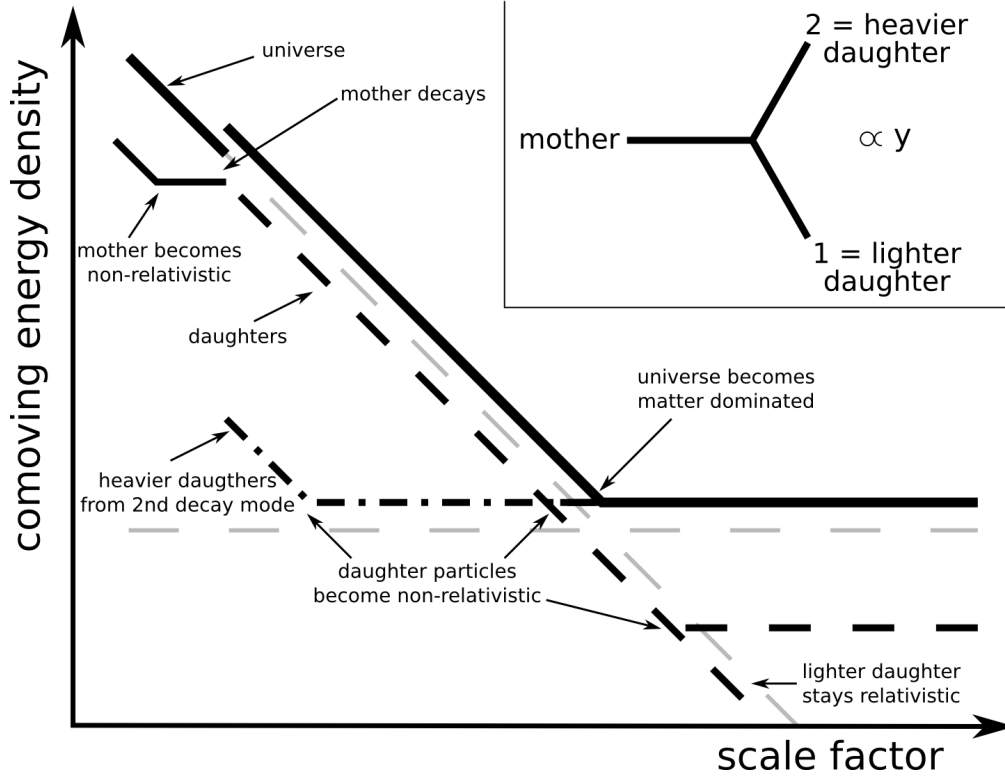


Figure 1: Behaviour of comoving energy densities  $\rho a^3$  in an expanding universe with dark radiation from particle decay. The full-logarithmic figure is illustrative and not exact. Upper right corner: Nomenclature for the considered two-body decay.

dark radiation as in [36]. Since only the relative behaviour matters, comoving energy densities  $\rho a^3$  are drawn. When the mother decays, its energy density is converted into the energy density of its relativistic daughters. The radiation content of the Universe is increased. Of course, there are various possible production mechanisms for the mother in the early universe. It is crucial only that its energy density is within a certain range at its decay, see below. The energy density of the daughters scales as radiation till they become non-relativistic. They may still be relativistic today or, especially, the heavier one may have become non-relativistic earlier and thus could possibly form the observed dark matter or some hot dark matter component. For comparison, the energy densities of radiation and matter in standard cosmology are shown as grey dashed curves.

If the decaying particle (mother) decays with some effective strength  $y$  into its decay products (daughters), an effective decay width might be given as  $\Gamma \sim y^2 m / (16\pi)$ , where  $m$  denotes the mass of the mother. For the following it is assumed that the branching ratio of this decay is close to one. Actually, we find in Sec. 3 that in all cases we are aware of the branching ratio into dark components is constrained to be very close to one at times later than  $t_{\text{BBN}} \sim 0.1$  s. Such branching ratios are common in dark matter models, because usually some symmetry is invoked to stabilise the dark matter candidate. In

the on-shell tree approximation some heavier particle sharing the symmetry then has to decay into the dark matter candidate. Such branching ratios may also –or in addition– be enforced by the mass spectrum allowing for only one decay channel kinematically.

A prime example for a dark matter stabilising symmetry is  $R$ -parity in supersymmetric models, which also naturally comprise extremely long-lived particles, if combined with gravity. Think about the gravitino decaying into axino and axion with effective  $y^2 \sim m_{3/2}^2/(12M_{\text{pl}}^2)$ , where  $m_{3/2}$  denotes the gravitino mass and  $M_{\text{pl}}$  the reduced Planck mass. This decay naturally leads to the emergence of dark radiation way after BBN but before photon decoupling [36]. The mother (= gravitino) would decay into a fermionic axino and an axion scalar. Another example is the decay of the lightest ordinary supersymmetric particle (LOSP) into its superpartner and the gravitino with effective  $y^2 \sim m_{\text{losp}}^4/(3M_{\text{pl}}^2 m_{3/2}^2)$ , where  $m_{\text{losp}}$  denotes the LOSP mass. The scenario reminds of the sWIMP mechanism, where these kind of decays were considered to produce the observed dark matter. In the case of a neutralino LOSP the mother were a fermion decaying into the fermionic gravitino and a gauge boson. In the case of a sneutrino LOSP the mother were a scalar and both daughters (= neutrino and gravitino) fermions. We mention a third example. In higher dimensional theories the superpartner of a modulus field, i.e., a modulino might decay with effective  $y^2 \sim \lambda m_{\tilde{\phi}}^2/(3M_{\text{pl}}^2)$ , where  $m_{\tilde{\phi}}$  denotes the modulino mass and  $\lambda$  an effective coupling. The modulino might decay into a sneutrino-neutrino or axino-axion pair and so on. Note that there are various combinations of spins.

## 2.1 Basics

We introduce useful parameters, determine general properties and derive basic equations.

**Kinematics** In the rest frame of the decaying particle the decay products of a two-body decay have in full generality momenta with opposite direction and same absolute value. It is

$$|\vec{p}_1| = |\vec{p}_2| = \frac{1}{2m} \left( (m^2 - (m_1 + m_2)^2)(m^2 - (m_1 - m_2)^2) \right)^{\frac{1}{2}}, \quad (1)$$

if  $m$  denotes the rest mass of the decaying particle and subscripts 1,2 label the two decay products. We choose subscripts such that  $m_1 < m_2$ . We find it useful to define

$$\delta \equiv \frac{m - m_2}{m_2} = \frac{m}{m_2} - 1 > 0 \quad (2)$$

as measure of the mass hierarchy between mother and the heavier daughter; or their mass degeneracy for  $\delta \lesssim 1$ . Negative  $\delta$  does not exist, because the decay were kinematically forbidden in that case. The mass of the heavier daughter can be written as

$$m_2 = (\delta + 1)^{-1} m. \quad (3)$$

If the decay shall produce dark radiation, the energy of the lighter decay product,  $E_1 = \sqrt{|\vec{p}_1|^2 + m_1^2}$ , must be dominated by its kinetic energy. For  $m_1 \ll |\vec{p}_1|$  its energy  $E_1 \simeq |\vec{p}_1|$ . In the limit  $m_1 \ll m_2$ , which is equal to  $m_1/m \ll (\delta + 1)^{-1}$ , the general

momentum (1) simplifies as

$$\lim_{m_1 \ll m_2} |\vec{p}_1| = \frac{m}{2} \frac{(\delta + 1)^2 - 1}{(\delta + 1)^2} = \frac{m}{2} \left( 1 - \frac{1}{(\delta + 1)^2} \right). \quad (4)$$

For the case  $m_1 = m_2$  see Sec. 4.

**On  $T_2^{\text{nr}}$**  An initial particle momentum  $p_{\text{ini}}$  from a decay at temperature  $T_d$  decreases due to the expansion of the Universe. Here and in the following, temperatures  $T$  refer to the corresponding photon temperature  $T_\gamma$  at the considered time, e.g.,  $T_d = T_\gamma(\tau) = T(\tau)$ . The momentum at temperature  $T$  is

$$p(T) = p_{\text{ini}} \frac{a_d}{a} = p_{\text{ini}} \frac{T}{T_d} \left( \frac{g_{*s}^d}{g_{*s}^d} \right)^{\frac{1}{3}}, \quad (5)$$

where  $a$  denotes the scale factor of the Universe and the second equality is due to the conservation of comoving entropy. As usual,  $g_{*s} = g_{*s}(T)$  is the effective number of degrees of freedom in the entropy density of the Universe  $s = (2\pi^2/45)g_{*s}T^3$ . The superscript on  $g_{*s}$  indicates here and in the following at which temperature or time  $g_{*s}$  is evaluated,  $g_{*s}^d \equiv g_{*s}(T_d)$ . The same holds for subscripts on  $a$ . We define the temperature  $T^{\text{nr}}$ , when a particle becomes non-relativistic, by

$$p(T^{\text{nr}}) = m, \quad (6)$$

where  $p \equiv |\vec{p}|$  denotes the particle's momentum and  $m$  its mass. For a particle species following the distribution  $P$  we consider the mean momentum to determine whether the species is relativistic or non-relativistic.

In our case  $p_{\text{ini}}$  is given by (4) and the mass of the heavier daughter by (3). Therefore, the condition

$$p_2(T_2^{\text{nr}}) \stackrel{!}{=} m_2 \quad (7)$$

yields

$$T_2^{\text{nr}} = T_d \frac{2}{\mu} \frac{\delta + 1}{(\delta + 1)^2 - 1} \left( \frac{g_{*s}^d}{g_{*s}^{\text{nr}}} \right)^{\frac{1}{3}} \quad (8)$$

with  $g_{*s}^{\text{nr}} = g_{*s}(T_2^{\text{nr}})$ . The correction factor  $\mu = c^{-1}\Gamma[c^{-1}]$  takes into account the exponential decay law in an expanding universe,  $a \propto t^{1/c}$ , compared to the sudden decay approximation. It is derived in Appendix A. It is  $\mu = \mu(P) \simeq 0.886$ , if the decay occurs during radiation domination and  $\mu \simeq 0.902$ , if the decay occurs during matter domination. Throughout this work we will often argue under the assumption of a sudden decay, because this simplifies the discussion and reveals key points. One example for this is whenever we consider some notion “at decay”. We will take into account corrections from the exponential decay law in the final equations by correction factors, which represent good approximations for times  $t \gtrsim 3\tau$  or  $\gtrsim 4\tau$ , cf. Appendix A. Often times of interest are indeed much later than the time of decay.

**Energy densities** The “non-dark” radiation energy density of the Universe, i.e., the energy density of the thermal bath in the Universe, is given by

$$\rho_{\text{rad}} = \frac{\pi^2}{30} g_* T^4, \quad (9)$$

where  $g_* = g_*(T)$  denotes the effective number of relativistic degrees of freedom in the bath. Bounds on the total radiation energy density  $\rho_{\text{rad}}^{\text{tot}}$  exist from processes around and after  $e^+e^-$ -annihilation, so for cosmic temperatures around and smaller than the  $e^+e^-$ -annihilation temperature  $T_{e^+e^-} \sim m_e \simeq 0.5$  MeV. They are usually given in terms of the effective number of neutrino species  $N_{\text{eff}}$  defined by

$$\rho_{\text{rad}}^{\text{tot}} = \left( 1 + N_{\text{eff}} \frac{7}{8} \left( \frac{T_\nu}{T_\gamma} \right)^4 \right) \rho_\gamma, \quad (10)$$

where the radiation energy density is given as a sum of the energy density in photons  $\rho_\gamma = (\pi^2/15)T^4$ , the energy density in SM neutrinos with  $N_{\text{eff}}^{\text{SM}} = 3.046$  [49] and  $T_\nu/T_\gamma = (4/11)^{1/3}$  and any departure from the standard scenario parametrised as a summand in  $N_{\text{eff}} = N_{\text{eff}}^{\text{SM}} + \Delta N_{\text{eff}}$ . The small correction in  $N_{\text{eff}}^{\text{SM}}$  is due to incomplete neutrino decoupling at  $e^+e^-$ -annihilation. We denote temperatures before neutrinos become non-relativistic at  $T_\nu^{\text{nr}}$  and lower than  $T_{e^+e^-}$  by  $T_{\text{low}}$ . Comparing (9) and (10) we see that  $g_*(T_{\text{low}}) \simeq 3.384$ .<sup>2</sup> In this temperature range the energy density in dark radiation  $\rho_{\text{dr}}$  can be written as

$$\rho_{\text{dr}} = \Delta N_{\text{eff}} \times \rho_{1\nu} = \Delta N_{\text{eff}} \times \frac{7}{8} \left( \frac{T_\nu}{T_\gamma} \right)^4 \rho_\gamma, \quad (11)$$

if  $\rho_{1\nu}$  denotes the energy density of one SM neutrino species with thermal spectrum. It follows that

$$\left. \frac{\rho_{\text{dr}}}{\rho_{\text{rad}}^{\text{SM}}} \right|_{\text{low}} = 0.1342 \times \Delta N_{\text{eff}} \quad (12)$$

for  $T_\nu^{\text{nr}} < T < T_{e^+e^-}$ . We see that even for the 5- $\sigma$  exclusion,  $\Delta N_{\text{eff}}^{\text{max}} = 5.265$ , of the combined analysis in [6], there would be less dark than SM radiation. Here and in the following a vertical line with subscripts like  $|_{\text{low}}$  indicates at what time (or temperature) the corresponding term is evaluated. Towards higher temperatures the bath energy density  $\rho_{\text{rad}} \propto g_* T^4$ , while the one in dark radiation scales as  $\rho_{\text{dr}} \propto g_{*s}^{4/3} T^4$ , if dark radiation is decoupled from the bath. Thus, at the time of the decay producing the dark radiation,

$$\left. \frac{\rho_{\text{dr}}}{\rho_{\text{rad}}} \right|_{\text{dec}} = \frac{\rho_{\text{dr}}(T_{\text{dec}})}{\rho_{\text{dr}}(T_{\text{low}})} \frac{\rho_{\text{rad}}^{\text{SM}}(T_{\text{low}})}{\rho_{\text{rad}}^{\text{SM}}(T_{\text{dec}})} \left. \frac{\rho_{\text{dr}}}{\rho_{\text{rad}}^{\text{SM}}} \right|_{\text{low}} = \left( \frac{g_{*s}^{\text{d}}}{g_{*s}^{\text{low}}} \right)^{\frac{4}{3}} \left( \frac{g_*^{\text{low}}}{g_*^{\text{d}}} \right) \left. \frac{\rho_{\text{dr}}}{\rho_{\text{rad}}^{\text{SM}}} \right|_{\text{low}}. \quad (13)$$

and inserting  $g_*(T_{\text{low}})$  and  $g_{*s}(T_{\text{low}}) = g_{*s}^0 = 2(1 + N_{\text{eff}}^{\text{SM}} 28/88) \simeq 3.938$  finally<sup>2</sup>

$$= 0.5440 \frac{(g_{*s}^{\text{d}})^{4/3}}{g_*^{\text{d}}} \left. \frac{\rho_{\text{dr}}}{\rho_{\text{rad}}^{\text{SM}}} \right|_{\text{low}}, \quad (14)$$

---

<sup>2</sup> The differences in  $g_*$  and  $g_{*s}$  to the often used values in the literature are due to the small correction in  $N_{\text{eff}}^{\text{SM}}$ .

which is valid at any decay temperature. Due to the different scaling behaviour the dark radiation component could have dominated the Universe at decay, but only for decays with  $g_* = g_{*s} \gg g_*^0$  and for extreme values of  $\Delta N_{\text{eff}}$ . At intermediate temperatures  $T$  we consider the different scaling of dark and SM radiation. It is

$$\rho_{\text{dr}}(T) = 0.0730 \Delta N_{\text{eff}} \frac{g_{*s}^{4/3}}{g_*} \rho_{\text{rad}}(T). \quad (15)$$

This is a useful parametrisation of the dark radiation energy density.

The desired amount of dark radiation determines the energy density of the decaying particle  $\rho = n m$  at its decay. In a two-body decay with branching ratio one the number densities of the decay products are fixed to be equal to the number density of the decaying particle,  $n = n_1 = n_2$ . As radiation the energy of a particle can be approximated by its momentum,  $E \simeq p$ , and the heavier daughter may act or may not act as dark radiation at the times of observation. Then the energy density of dark radiation at decay reads  $\rho_{\text{dr}}|_{\text{dec}} \simeq g_{\text{dr}}^{\text{obs}} n E_1 \simeq g_{\text{dr}}^{\text{obs}} n p_1$ , where  $p_1$  is determined from the kinematics (4) and  $g_{\text{dr}}^{\text{obs}}$  counts the number of dark radiation components at the time of observation. It is  $g_{\text{dr}} = 2$  or 1, if the heavier daughter particle became non-relativistic before the time probed by observations. We define a conversion factor  $f$  by

$$\rho_{\text{dr}} = f \times \rho \quad (16)$$

so that

$$f = \mu \frac{g_{\text{dr}}^{\text{obs}}}{2} \frac{(\delta + 1)^2 - 1}{(\delta + 1)^2}. \quad (17)$$

The factor  $\mu$  takes into account the exponential decay law in an expanding Universe, see Appendix A. Altogether, we obtain

$$\left. \frac{\rho}{\rho_{\text{rad}}} \right|_{\text{dec}} = f^{-1} \left. \frac{\rho_{\text{dr}}}{\rho_{\text{rad}}} \right|_{\text{dec}} = \frac{0.146}{\mu} \frac{\Delta N_{\text{eff}}}{g_{\text{dr}}^{\text{obs}}} \frac{(g_{*s}^{\text{d}})^{4/3}}{g_*^{\text{d}}} \frac{(\delta + 1)^2}{(\delta + 1)^2 - 1}. \quad (18)$$

We see that the decaying particle could be required to dominate the energy density of the Universe for a short time prior its decay to explain extreme values of  $\Delta N_{\text{eff}}$ . However, this is not to be expected and, especially, at late times improbable. The dilution relative to  $\rho_{\text{rad}}$  is only  $\propto g_*^{1/3}$ , so that a large number  $g_* \gg g_*^{\text{SM}}$  would be necessary to change this. From (18) follows today's energy density of the decaying particle, if it were not decayed, in units of today's critical energy density  $\rho_c$  as

$$\Omega h^2 = \frac{\rho|_{\text{dec}} h^2}{\rho_c} \left( \frac{T_0}{T_{\text{d}}} \right)^3 \frac{g_{*s}^0}{g_{*s}^{\text{d}}}, \quad (19)$$

where the dilution till today, that would have happened, is considered. In this work we will heavily use the fact that the energy density of the decaying particle is fixed by the amount of dark radiation and thus by observations independent of an underlying particle physics model. The other way around we can single out  $\Delta N_{\text{eff}}$  in (18) resulting in

$$\Delta N_{\text{eff}} = 9.13 \mu \frac{m Y}{T_{\text{d}}} \frac{(\delta + 1)^2 - 1}{(\delta + 1)^2} \frac{g_{\text{dr}}^{\text{obs}}}{(g_{*s}^{\text{d}})^{1/3}}, \quad (20)$$



where we introduced the particle yield  $Y = n/s$ .

If the decay occurs before BBN,  $\tau \ll t_{\text{BBN}}$ , the decaying particle may dominate the Universe prior its decay. In this case  $\Delta N_{\text{eff}}$  is set by the relative branching into radiation formed by SM particles and dark radiation. This relative branching is just found in (15), i.e.  $0.073 \Delta N_{\text{eff}} g_*^{1/3}$ .

## 2.2 $\delta$ - $\tau$ plane

The mass hierarchy between decaying particle and decay products is constrained from several cosmological considerations. First of all, at no time there is an upper bound on  $\delta$ , because the energy density of the decaying particle can, in principle, be adjusted such that all its energy transferred to radiation at its decay accounts for the desired increase in  $\Delta N_{\text{eff}}$ . This might be different in a concrete particle physics model, where  $\delta$  and/or  $\rho$  turn out to be given. More importantly, there are lower bounds on  $\delta$  from cosmology. The underlying considerations are qualitatively different, if the decay occurs before or after matter-radiation equality at  $t_{\text{eq}}$ . In any case they depend on the time of decay  $\tau$ , while they are independent of the underlying particle physics model. Our assumptions on the time and temperature of equality are outlined at the beginning of Sec. 2.3.

**Before**  $t_{\text{eq}}$  there is a lower bound on  $\delta$  from the requirement that no daughter particle may come to dominate the Universe before  $t_{\text{eq}}$ . This non-dominance requirement can be expressed as

$$\Omega_2 h^2 = b_{\text{max}} \Omega_{\text{dm}} h^2 \quad (21)$$

with  $b_{\text{max}} \leq 1$ . When the mother decays (not too close before  $t_{\text{eq}}$ ) also the heavier daughter particle must be emitted as radiation. Otherwise, it would dominate already shortly after being emitted. Thus its energy density is as large as the energy density of the lighter daughter,  $\rho_2|_{\text{dec}} = \rho_1|_{\text{dec}} = (g_{\text{dr}}^{\text{obs}})^{-1} \rho_{\text{dr}}(T_{\text{d}})$ . After emission its energy density scales as radiation  $\propto a^{-4}$  till it becomes non-relativistic at  $T_2^{\text{nr}}$ . If  $T_2^{\text{nr}} < T_{\text{eq}} \Leftrightarrow t_2^{\text{nr}} > t_{\text{eq}}$ ,  $\rho_2$  surely never dominates. From becoming non-relativistic on it scales as matter  $\propto a^{-3}$ . Thus

$$\Omega_2 = \frac{\rho_{\text{dr}}(T_{\text{d}})}{\rho_{\text{c}}} (g_{\text{dr}}^{\text{obs}})^{-1} \frac{T_2^{\text{nr}} T_0^3}{T_{\text{d}}^4} \left( \frac{g_{*s}^0}{g_{*s}^{\text{d}}} \right)^{\frac{4}{3}}, \quad (22)$$

where we anticipated  $g_{*s}^{\text{nr}} = g_{*s}^0$ . Inserting  $\rho_{\text{dr}}$  from (15) the inequality (21) becomes an upper bound on  $T_2^{\text{nr}}$

$$T_2^{\text{nr}} \leq 6.938 T_{\text{eq}} \Delta N_{\text{eff}}^{-1} b_{\text{max}} \frac{\Omega_{\text{dm}} h^2}{0.1246} g_{\text{dr}}^{\text{obs}} \quad (23)$$

where we can see that for the bound only  $g_{\text{dr}}^{\text{obs}} = 1$  is sensible. Since  $T_2^{\text{nr}} \ll T_{e^+e^-}$ , it is justified to set  $g_*^{\text{nr}} = g_*^0$ . We find the corresponding cosmic time as

$$(t_2^{\text{nr}})_{\text{min}} = 0.0254 t_{\text{eq}} b_{\text{max}}^{-1} \Delta N_{\text{eff}}^2 \left( \frac{0.1246}{\Omega_{\text{dm}} h^2} \right)^2 = 4.61 \times 10^{10} \text{ s } b_{\text{max}}^{-1} \Delta N_{\text{eff}}^2 \left( \frac{0.1246}{\Omega_{\text{dm}} h^2} \right)^2. \quad (24)$$

For times later than  $(t_2^{\text{nr}})_{\text{min}}$  the assumption of relativistic emission is no longer necessarily fulfilled. We note that  $t_2^{\text{nr}}$  from (23) is likely later than the time when the first

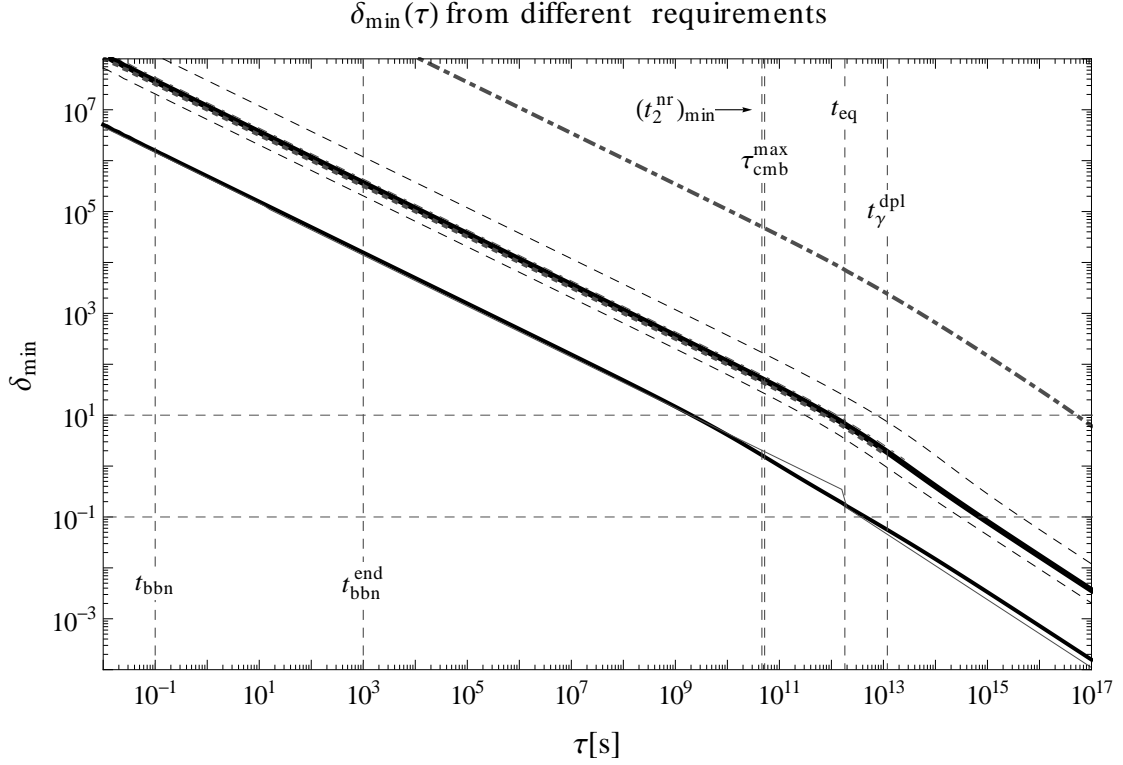


Figure 2:  $\delta_{\min}$ - $\tau$ -plane exploiting (25). Values above the corresponding line are considered to be allowed. The thick solid curve corresponds to the hot dark matter constraint, cf. Sec. 2.3.2, with  $\Delta N_{\text{eff}} = 1$ . Thin dashed curves below ( $\Delta N_{\text{eff}} = 0.52$ ) and above ( $\Delta N_{\text{eff}} = 5.265$ ) show the dependence of this bound on the produced amount of dark radiation. The thin solid curve corresponds to the non-domination constraint. The dotted curve (at the lower edge of the thick solid one) gives  $\delta$  such that the heavier daughter becomes non-relativistic at photon decoupling  $t_{\gamma}^{\text{dpl}}$  and the dash-dotted one such that this happens today. These three curves are for  $\Delta N_{\text{eff}} = 1$ . At the upper edge of the thick solid curve mean values of [48] originate from the decay for massless neutrinos. Various important and suggestive times are highlighted by vertical dashed lines: onset  $t_{\text{bbn}}$  and end of BBN  $t_{\text{bbn}}^{\text{end}}$ , the earliest possible time for the heavier daughter to become non-relativistic  $(t_2^{\text{nr}})_{\min}$  from (24), re-entry of first observable modes in the CMB  $\tau_{\text{cmb}}^{\text{max}}$  and matter-radiation equality  $t_{\text{eq}}$ . For decays during BBN the increase in  $N_{\text{eff}}$  determined from BBN is smaller than the corresponding increase measured in the CMB. The relative difference depends on the time of decay as quantified in [38]. In all figures we take into account the evolution of  $g_*$  and  $g_{*s}$ . That the curves are smooth around  $t_{e^+e^-}$  shows that dependencies have cancelled. Within the horizontal dashed lines the mass hierarchy or degeneracy is within an order of magnitude.

observable modes of the CMB enter the horizon, which sets  $\tau_{\text{cmb}}^{\text{max}} \simeq 5.2 \times 10^{10} \text{ s}$  [35]. Indeed, this is for sure taking into account constraints from structure formation requiring  $b_{\text{max}} < 1$ , cf. Sec. 2.3. The heavier daughter is restricted to become non-relativistic during CMB times or later, which might leave observable consequences due to the corresponding change in the expansion rate.

Inserting  $T_2^{\text{nr}}$  from (8) in (23) we obtain an implicit lower bound on  $\delta$

$$\frac{(\delta + 1)^2 - 1}{\delta + 1} > \frac{0.2883}{\mu} \frac{T_{\text{d}}}{T_{\text{eq}}} \Delta N_{\text{eff}} \left( \frac{0.1246}{\Omega_{\text{dm}} h^2} \right) \left( \frac{g_{*s}^{\text{d}}}{g_{*s}^0} \right)^{\frac{1}{3}}. \quad (25)$$

If  $\delta \gg 1$ , the lhs of (25) reduces as

$$\lim_{\delta \rightarrow \infty} \frac{1}{\delta} \frac{(\delta + 1)^2 - 1}{\delta + 1} = 1. \quad (26)$$

Then (25) becomes practically

$$\delta > \frac{0.2883}{\mu} \left( \frac{t_{\text{eq}}}{\tau} \right)^{\frac{1}{2}} \Delta N_{\text{eff}} \left( \frac{0.1246}{\Omega_{\text{dm}} h^2} \right) \left( \frac{g_{*}^0}{g_{*}^{\text{d}}} \right)^{\frac{1}{4}} \left( \frac{g_{*s}^{\text{d}}}{g_{*s}^0} \right)^{\frac{1}{3}}, \quad (27)$$

where we used the time-temperature relation in a radiation dominated universe to replace  $T_{\text{d}}/T_{\text{eq}} = (g_{*}^{\text{eq}}/g_{*}^{\text{d}})^{1/4} (t_{\text{eq}}/\tau)^{1/2}$  and  $g_{*}^{\text{eq}} = g_{*}^0$ .

**After**  $t_{\text{eq}}$  a relativistically emitted, non-dominating particle becomes even more subdominant as the Universe expands. However, there is a lower bound on  $\delta$ , if we require some significant  $\Delta N_{\text{eff}} > 0$ , because the maximally allowed energy density for the heavier daughter particle is the dark matter energy density as (21) with the crucial difference that it is emitted non-relativistically, here. When  $b \simeq 1$ , dark matter would decay and convert a small amount of its energy into radiation. This is qualitatively different for  $\tau < (t_2^{\text{nr}})_{\text{min}}$ . In the intermediate regime,  $(t_2^{\text{nr}})_{\text{min}} < \tau \lesssim t_{\text{eq}}$ , we expect observable consequences in the CMB.

The energy density of a non-relativistic,  $p_2 < m_2$ , species can be approximated as  $\rho_2 = n_2 E_2 \simeq n_2 m_2$ . Again exploiting  $n = n_2 = n_1$  and replacing  $m_2$  by (3) we find

$$\rho_2 = \frac{n m}{\delta + 1} \Rightarrow \rho_2|_{\text{d}} = (\delta + 1)^{-1} f^{-1} \rho_{\text{dr}}(T_{\text{d}}), \quad (28)$$

where we used that  $\rho = nm$  and the definition of the conversion factor (16). Taking into account the red-shift till today the energy density of the heavier daughter in units of today's critical energy density is given by

$$\Omega_2 h^2 = \frac{2}{\mu} \frac{\delta + 1}{(\delta + 1)^2 - 1} \frac{\rho_{\text{dr}}(T_{\text{d}}) h^2}{\rho_{\text{c}}} \left( \frac{T_0}{T_{\text{d}}} \right)^3. \quad (29)$$

From the requirement (21) we obtain the very same implicit lower bound (25) on  $\delta$  for decays after  $(t_2^{\text{nr}})_{\text{min}}$ , where only  $g_{*s}^{\text{d}}/g_{*s}^0$  has to be replaced by one. If  $\delta \rightarrow 0$ , the lhs of (25) reduces as

$$\lim_{\delta \rightarrow 0} \frac{1}{2\delta} \frac{(\delta + 1)^2 - 1}{\delta + 1} = 1. \quad (30)$$

Then (25) becomes practically

$$\delta > \frac{0.2883}{2\mu} \left( \frac{t_{\text{eq}}}{\tau} \right)^{\frac{2}{3}} \Delta N_{\text{eff}} \left( \frac{0.1246}{\Omega_{\text{dm}} h^2} \right), \quad (31)$$

where we used the time-temperature relation in a matter dominated universe with constant  $g_*$  to replace  $T_{\text{d}}/T_{\text{eq}} = (t_{\text{eq}}/\tau)^{\frac{2}{3}}$ . Whenever necessary we assume a sudden transition from radiation to matter domination in analytic calculations.

The lower bound on  $\delta$  from (25) with  $\Delta N_{\text{eff}} = 1$  is depicted in Fig. 2 as thin solid curve. The analytic approximations (27) and (31) are overplotted as very thin grey curve with a jump and its largest deviation at  $t_{\text{eq}}$  and a tiny underestimation at very late times. A decay before  $t_{\text{bbn}}$  increases  $\Delta N_{\text{eff}}$  before BBN. We found that the decay products may not become non-relativistic before a time  $(t_2^{\text{nr}})_{\text{min}} > \tau_{\text{cmb}}^{\text{max}}$ . For decays during BBN the increase in  $N_{\text{eff}}$  determined from BBN is smaller than the increase measured in the CMB depending on the time of decay [38]. Decays after  $t_{\text{bbn}}^{\text{end}}$  add radiation during CMB times. It is usually assumed that the decay products are still relativistic today or at least till photon decoupling at  $t_{\gamma}^{\text{dpl}}$ , while this must not be the case, especially not for the heavier daughter. The figure ranges beyond  $t_{\gamma}^{\text{dpl}}$  to times as late as  $10^{17}$  s. This is for completeness. We point out that for such late decays the meaning of the curve is maybe far from clear in this and other following graphs. This is due to the currently limited understanding. Nevertheless, first pieces of information are provided that might motivate focused studies of such cosmologies.

Finally, let us give the following comment. We could have started from the general requirement (21) for any time and would have obtained the same results. We would like repeat that the cosmology is very different for a decay close to the boundary occurring sufficiently before or after  $(t_2^{\text{nr}})_{\text{min}}$ . After  $(t_2^{\text{nr}})_{\text{min}}$  the energy density of the decaying particle is of the order of the energy density of the heavier daughter. In some sense dark matter decays into today's dark matter particle and dark radiation. Before  $(t_2^{\text{nr}})_{\text{min}}$  the energy density of the decaying particle has to be much larger than the dark matter energy density to produce significant dark radiation. One could expect a lower bound on  $\delta$  from requiring some significant  $\Delta N_{\text{eff}}$  to arise also before  $(t_2^{\text{nr}})_{\text{min}}$ . However, this is not the case. The energy density of the decaying particle could in principle be arbitrarily large, such that in its decay a tiny amount of its energy converted into dark radiation suffices. This is because dark radiation does not thermalise and thus does not dilute pre-existing abundances. The additional entropy is negligible as the momenta of the decay products are distributed on a small shell in phase space, cf. Appendix A. An arbitrarily small  $\delta$  seems allowed. Indeed, the non-dominance requirement of (21) were violated. For  $\delta$ s fulfilling (25) the upper bound on the energy density of the decaying particle is set by the possible overproduction of dark radiation, so a too large increase in  $\Delta N_{\text{eff}}$  inconsistent with observations. In the scenario under consideration this upper bound were set via (18). The lower bound on  $\delta$  requiring some minimal  $\Delta N_{\text{eff}}$  is obtained by inserting this value into (25). For times around  $t_{\text{eq}}$  the situation is more involved than outlined, here, because quite a large fraction of the dominating matter component would have to decay into radiation. However, we expect such a situation to leave pronounced signatures in the CMB.

### 2.3 Structure formation

The transition from radiation to matter domination is one of the most important events in structure formation. The red-shift of matter-radiation equality  $z_{\text{eq}}$  is related to the dark radiation and matter density  $\Omega_{\text{m}}$  by (cp. (53) of [50])

$$1 + z_{\text{eq}} = 3201 \left( \frac{\Delta N_{\text{eff}}}{7.45} + 1 \right)^{-1} \frac{\Omega_{\text{m}} h^2}{0.1333}. \quad (32)$$

Naively, one could conclude that  $\Delta N_{\text{eff}} > 0$  thus implies smaller  $z_{\text{eq}}$ , i.e. a later transition. However, this is not observed. Primordial abundances of light nuclei are simply affected by the expansion rate during BBN, which is given by the amount of radiation and thus  $N_{\text{eff}}$ . What can be seen in the CMB power spectrum is a suppression at higher multipoles (corresponding to smaller scales) compared to the expectation from the standard scenario. Constraints on  $N_{\text{eff}}$  depend on the cosmological model, which can be extended in other ways to suppress small-scale power. For an increase in  $N_{\text{eff}}$  the suppression has been identified to be due to increased Silk damping caused by the increased expansion rate [7]. Indeed, (32) shows the degeneracy of  $N_{\text{eff}}$  and  $\Omega_{\text{m}} h^2$ , in particular, for WMAP using the first and third acoustic peak to determine  $z_{\text{eq}}$ . This degeneracy is broken by including measurements on smaller scales. The combined data then allows to measure  $N_{\text{eff}}$  in addition to  $z_{\text{eq}}$ , see references in the introduction. The studies do not find that  $z_{\text{eq}}$  varies with  $\Delta N_{\text{eff}}$ . Even though they also do not exclude a smaller  $z_{\text{eq}}$ , we adopt the PDG mean value  $z_{\text{eq}} = 3200 \pm 130$  [51], which is consistent with the other studies. The temperature at equality is thus  $T_{\text{eq}} = (1 + z_{\text{eq}})T_0 \approx 0.752$  eV. We fix the time of matter-radiation equality to  $t_{\text{eq}} \approx 1.81 \times 10^{12}$  s from the relation between time and red-shift in a universe filled with radiation and matter using PDG mean values for the time and red-shift of decoupling [51].

For a fixed  $z_{\text{eq}}$  the matter and radiation density are no longer independent. In Fig. 1 this might be seen comparing the energy density of the Universe including dark radiation (thick, solid) with standard cosmology (grey, dashed). The baryon density is regarded as robustly measured,  $\Omega_{\text{b}} h^2 = 0.0226(6)$  with  $1\sigma$  uncertainty in the last digit [51]. Therefore, the uncertainty in  $\Delta N_{\text{eff}}$  turns into an uncertainty in the dark matter density as  $\Omega_{\text{m}} = \Omega_{\text{b}} + \Omega_{\text{dm}}$ . Following (32) dark matter and dark radiation energy densities are linked as

$$\Omega_{\text{dm}} h^2 = 0.1067 + 0.0179 \Delta N_{\text{eff}}. \quad (33)$$

Omitting this dependence in, for example, Sec. 2.2 can lead to deviations up to few ten percent. Thus it is important to take this dependence into account. This is especially true when considering more complete cosmologies including, for example, an origin of dark matter as in Sec. 4. Particle physics parameters can be significantly affected. An example might be the determination of the relic density of the lightest supersymmetric particle in supersymmetric models.

Increasing the dark matter energy density, while keeping the baryon density constant, decreases the baryonic matter fraction  $\Omega_{\text{b}}/\Omega_{\text{m}}$ . This decreases the pressure support on matter prior to photon decoupling and, therefore, boosts the growth of structures below the sound horizon at photon decoupling of about 150 Mpc [52]. A finite neutrino

mass scale has the opposite effect, because neutrinos then count to  $\Omega_m$ , while they do not take part in structure formation below their free-streaming scale. Consequently, a best-fit might be found having both, additional radiation and a –small, “compensating”– dark matter fraction with very large free-streaming scale, see [53, 54] considering sterile neutrinos. In this line of thought it is very interesting that  $\Delta N_{\text{eff}} > 0$  together with a finite neutrino mass scale seems to be favoured by measurements of the abundance of galaxy clusters corresponding to  $\sim 10$  Mpc scales [48]. We note that all these considerations assume a decay before the affected epoch, so for example before  $t_{\text{eq}}$  to increase the amount of radiation at  $t_{\text{eq}}$  and so on. It is neither clear how an increase in  $N_{\text{eff}}$  after  $t_{\gamma}^{\text{dpl}}$  might be observed nor what is the effect of the corresponding amount of matter being transformed into radiation. Also in this sense some figures range beyond  $t_{\gamma}^{\text{dpl}}$  for completeness only.

In the following we shall point out the constraints and opportunities arising from the heavier daughter in structure formation. It may constitute just half of the dark radiation, but it does not need to act as radiation at all. The opposite extreme case would be that the heavier daughter forms the observed dark matter. In between these two cases its free-streaming could mimic the finite neutrino mass scale as deduced from cosmological observations.

### 2.3.1 Minimal free-streaming scale

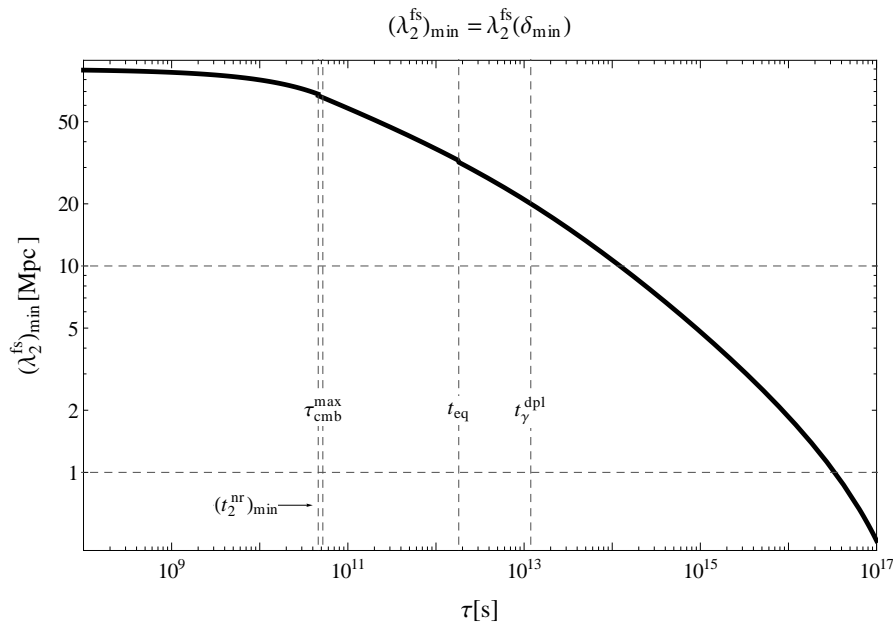


Figure 3: Minimal free-streaming scale of the heavier daughter  $(\lambda_2^{\text{fs}})_{\text{min}}$  depending on the time of decay. Times are highlighted as in Fig. 2. Horizontal dashed lines indicate the galaxy cluster scale  $\lambda_{\text{gc}} \sim 10$  Mpc and 1 Mpc as suggestive free-streaming scale of warm dark matter, respectively.

As collisionless particle the heavier daughter can stream out of overdense regions and into underdense regions, in the process smoothing out inhomogeneities. In order to take this effect into account properly, one should integrate Boltzmann equations. In the following we shall estimate the scale of collisionless damping analytically. The decisive quantity is the free-streaming scale

$$\lambda_2^{\text{fs}} \equiv \int_{\tau}^{t_0} \frac{v_2(a)}{a} dt \quad (34)$$

of the heavier daughter, where  $v(a)$  denotes scale factor dependent velocities. The situation is qualitatively different whether the decay occurs before or after  $(t_2^{\text{nr}})_{\text{min}}$ .

**Before  $(t_2^{\text{nr}})_{\text{min}}$**  both decay products are emitted relativistically. If a particle becomes non-relativistic after  $t_{\text{eq}}$ , its free-streaming scale is much larger than the size of a protogalaxy. It is said to act as hot dark matter, see Sec. 2.3.2. We will be interested in the case used in Sec. 2.2 to determine  $\delta_{\text{min}}$  where the heavier daughter becomes non-relativistic before  $t_{\text{eq}}$ . We approximate the velocity of a particle emitted with relativistic momentum by

$$v(a) \approx \begin{cases} 1 & , \text{if } a < a_{\text{nr}} \\ \frac{a_{\text{nr}}}{a} & , \text{if } a \geq a_{\text{nr}} . \end{cases} \quad (35)$$

After the emission with  $v \simeq 1$  the velocity decreases with the expansion of the Universe and becomes smaller than one, when the particle becomes non-relativistic at  $a_{\text{nr}}$ . A finite, non-relativistic velocity of the decaying particle is safely negligible. Exploiting the additivity of integration on intervals we thus find

$$\lambda_{\text{fs}} \approx \int_{\tau}^{t_{\text{nr}}} \frac{1}{a} dt + \int_{t_{\text{nr}}}^{t_{\text{eq}}} \frac{a_{\text{nr}}}{a^2} dt + \int_{t_{\text{eq}}}^{t_0} \frac{a_{\text{nr}}}{a^2} dt . \quad (36)$$

The first integral corresponds to relativistic free-streaming, the second one to non-relativistic free-streaming before  $t_{\text{eq}}$  and the third to non-relativistic free-streaming during the matter dominated era. We can safely neglect the current vacuum dominated phase.

In order to perform the integration analytically we take  $g_*$  and  $g_{*s}$  to be constant for times as late as  $t_{\text{nr}}$ . As the variation of  $g_{*s}^{1/3}$  and  $g_*^{1/4}$  with time is weak, we treat them like constant factors in the first integral, too. We checked numerically that this comes with negligible errors. With the additional approximation of a sudden transition between radiation and matter domination at  $t_{\text{eq}}$  the integrations become straightforward exploiting the common  $a(t)$  relations. We obtain

$$\lambda_{\text{fs}} \approx 2 \frac{\tau^{\frac{1}{2}} t_{\text{nr}}^{\frac{1}{2}}}{a_{\text{d}}} \left( \frac{g_{*s}^{\text{nr}}}{g_{*s}^{\text{d}}} \right)^{\frac{1}{3}} \left( \frac{g_*^{\text{d}}}{g_*^{\text{nr}}} \right)^{\frac{1}{4}} \left( 1 - \left( \frac{\tau}{t_{\text{nr}}} \right)^{\frac{1}{2}} \right) + \frac{t_{\text{nr}}}{a_{\text{nr}}} \left( 3 + \ln \frac{t_{\text{eq}}}{t_{\text{nr}}} \right) \quad (37)$$

with  $g_{*s}^{\text{nr}} = g_{*s}(t_{\text{nr}})$  and  $g_*^{\text{nr}} = g_*(t_{\text{nr}})$ . The first term corresponds to relativistic free-streaming, the first summand in the brackets of the second term to non-relativistic free-streaming during the matter dominated era and the logarithm to non-relativistic free-streaming before  $t_{\text{eq}}$ . Accepting an error of percent we have taken  $(t_{\text{eq}}/t_0)^{1/3} \rightarrow 0$  in the

last integral. In (37) we can see that for the often discussed case  $\tau \ll t_{\text{nr}} \ll t_{\text{eq}}$  relativistic free-streaming is negligible and non-relativistic free-streaming before  $t_{\text{eq}}$  dominates over free-streaming after  $t_{\text{eq}}$ . In this case  $\lambda_{\text{fs}}$  is roughly set by  $t_{\text{nr}}$ . In order to investigate our case we set  $t_{\text{nr}} = t_2^{\text{nr}} = t(T_2^{\text{nr}})$  in (37). The scale factors at corresponding times are given by  $a_{\text{d}} = a_0(T_0/T_{\text{d}})(g_{*s}^0/g_{*s}^{\text{d}})^{1/3}$  and  $a_{\text{nr}} = a_0(T_0/T_2^{\text{nr}})(g_{*s}^0/g_{*s}^{\text{nr}})^{1/3}$ , respectively. Since  $T_2^{\text{nr}}$  is given by (8) we can express the free-streaming scale of the heavier daughter as function of  $\delta$  and the time of decay  $\tau$ . We find

$$\begin{aligned} \lambda_2^{\text{fs}}(\delta, \tau) \approx & 0.09 \text{ Mpc} \left( \frac{\tau}{10^7 \text{ s}} \right)^{\frac{1}{2}} \frac{(\delta+1)^2 - 1}{\delta+1} \frac{(g_*^{\text{d}})^{1/4}}{(g_*^{\text{nr}})^{1/2}} \left( \frac{(g_{*s}^{\text{nr}})^2}{g_{*s}^{\text{d}} g_{*s}^0} \right)^{\frac{1}{3}} \\ & \times \left\{ 5 - \frac{4}{\mu} \frac{\delta+1}{(\delta+1)^2 - 1} \left( \frac{g_*^{\text{nr}}}{g_*^{\text{d}}} \right)^{\frac{1}{4}} \left( \frac{g_{*s}^{\text{d}}}{g_{*s}^{\text{nr}}} \right)^{\frac{1}{3}} \right. \\ & \left. + \ln \left[ \frac{t_{\text{eq}}}{\tau} \frac{4}{\mu^2} \left( \frac{\delta+1}{(\delta+1)^2 - 1} \right)^2 \left( \frac{g_*^{\text{nr}}}{g_*^{\text{d}}} \right)^{\frac{1}{2}} \left( \frac{g_{*s}^{\text{d}}}{g_{*s}^{\text{nr}}} \right)^{\frac{2}{3}} \right] \right\}. \end{aligned} \quad (38)$$

This analytic approximation applies to any case with  $\tau < t_{\text{nr}} < t_{\text{eq}} \ll t_0$ . Of course, as  $\tau \rightarrow t_{\text{nr}}$  there is no relativistic free-streaming.

The minimal free-streaming scale of the heavier daughter  $(\lambda_2^{\text{fs}})_{\text{min}}$  is indeed independent of the time of decay. It is instead given by the earliest possible time for the heavier daughter to become non-relativistic (23), which corresponds to the lowest possible initial velocity. It is achieved for minimal  $\delta$  given in (25), because for the minimally required mass hierarchy the heavier daughter is emitted with its minimally allowed initial momentum. We find

$$\begin{aligned} (\lambda_2^{\text{fs}})_{\text{min}}(\Delta N_{\text{eff}}, \tau) \approx & 9.9 \text{ Mpc} \Delta N_{\text{eff}} \left( \frac{0.1246}{\Omega_{\text{dm}} h^2} \right) \\ & \times \left( 5 - 2 \left( \frac{\tau}{(t_2^{\text{nr}})_{\text{min}}} \right)^{\frac{1}{2}} + \ln \left[ 48 \left( \Delta N_{\text{eff}}^{-1} \frac{\Omega_{\text{dm}} h^2}{0.1246} \right)^2 \right] \right). \end{aligned} \quad (39)$$

Consequently it depends on the amount of dark radiation only, except for the relativistic free-streaming scale in the first line. It is independent of  $g_*$  and  $g_{*s}$  at decay. Taking  $\Delta N_{\text{eff}} = 1$  and the limit  $\tau \ll t_{\text{nr}}$  we obtain  $(\lambda_2^{\text{fs}})_{\text{min}} \approx 89 \text{ Mpc}$  as shown in Fig. 3, which should be compared to the galaxy cluster scale  $\lambda_{\text{gc}} \sim 10 \text{ Mpc}$ . It is actually roughly a factor of nine larger. Thus the heavier daughter from a decay before  $(t_2^{\text{nr}})_{\text{min}}$  is in any case way too warm to form the observed dark matter, see below.

**After**  $t_{\text{eq}}$  to act as matter the heavier daughter should be emitted non-relativistically. We approximate its velocity by

$$v_2(a) \approx \frac{p_{\text{ini}}}{m_2} \frac{a_{\text{d}}}{a}, \quad (40)$$

where  $p_{\text{ini}}$  is given by (4). With  $a \propto t^{2/3}$  in a matter dominated universe the scale factor at decay  $a_{\text{d}} = (\tau/t_0)^{2/3}$  and the integration in (34) becomes straightforward. The free-streaming scale of the heavier daughter for  $\tau > t_{\text{eq}}$  reads

$$\lambda_2^{\text{fs}}(\delta, \tau) = 179 \text{ Mpc} \left( \frac{\tau}{10^{13} \text{ s}} \right)^{\frac{1}{3}} \frac{(\delta+1)^2 - 1}{\delta+1} \left( 1 - 0.0285 \left( \frac{\tau}{10^{13} \text{ s}} \right)^{\frac{1}{3}} \right), \quad (41)$$



where, now,  $\delta$ s are smaller than one in any case. Inserting the minimal  $\delta$  from (25) we obtain the minimal free-streaming scale of the heavier daughter  $(\lambda_2^{\text{fs}})_{\text{min}}$  for  $\tau > t_{\text{eq}}$ . It is depicted in Fig. 3. For decays occurring in the small window after  $(t_2^{\text{tr}})_{\text{min}}$  but before  $t_{\text{eq}}$  the curve in Fig. 3 represents a lower bound, because we did not consider that the Universe is radiation dominated in this period. However, around this time, for example, the assumption of sudden transitions leads to quite large errors in the estimate. We find that a correction were small and thus not important for our purpose.

Lyman- $\alpha$  forest data constrains the scale of collisionless damping. Constraints range between  $\lambda_{\text{fs}} \lesssim 0.5$  Mpc [55, 56], tighter ones [57] and those more relaxed due to the rejection of less reliable data [58, 57, 59]. We assume a constraint on the free-streaming scale  $\lambda_{\text{fs}} \lesssim 1$  Mpc to apply, if all the dark matter originates from particle decay. Since  $(\lambda_2^{\text{fs}})_{\text{min}} > \lambda_{\text{gc}} \sim 10$  Mpc  $\gg 1$  Mpc the bound (21) from non-dominance with  $b = 1$  is naive. The actual lower bound on  $\delta$  lies closer to the hot dark matter (HDM) bound of Sec. 2.3.2 with  $b_{\text{max}} < 1$ , cp. [59]. The heavier daughter from a two-body decay producing the desired dark radiation cannot form the observed dark matter. The HDM bound is the tightest bound obtainable taking into account the impact of the scenario on structure formation.

**Minimal velocity today** Using (5) we can compute today's velocity  $v^0$  of the decay products. Either a daughter is still relativistic,  $p > m \Rightarrow v \simeq 1$ , or has become non-relativistic,  $p < m \Rightarrow v \simeq p/m$ . With (4) and (3) we obtain for the heavier daughter

$$v_2^0(T_{\text{d}}, \delta) = \frac{T_0}{T_{\text{d}}} \frac{\phi}{2} \frac{(\delta + 1)^2 - 1}{\delta + 1} \left( \frac{g_{*s}^0}{g_{*s}^{\text{d}}} \right)^{\frac{1}{3}}, \quad (42)$$

where  $\phi$  denotes the variance of the probability distribution derived in Appendix A. It is  $\phi \simeq 0.215$  if the decay occurs during radiation domination and  $\phi \simeq 0.376$  if the decay occurs during matter domination. Bounds on today's dark matter velocity assume a Fermi-Dirac distribution, while the decay products are distributed as derived in Appendix A. While a transfer function is known [60], both distributions can be considered as having an equivalent effect on structure formation as long as they have an identical second moment of the distribution ( $\equiv$  variance), i.e. an identical root-mean-square velocity [61]. The factor  $\phi$  in (42) takes into account the exponential decay law in comparison to the sudden decay approximation. The minimal velocity of the heavier daughter today is obtained by inserting the lower bounds on  $\delta$  from Sec. 2.2 into (42). We find

$$(v_2^0)_{\text{min}} \simeq 3.3 \frac{\text{km}}{\text{s}} \frac{\phi(\tau)}{\phi(\tau \ll t_{\text{eq}})} \Delta N_{\text{eff}} \left( \frac{0.1246}{\Omega_{\text{dm}} h^2} \right) \left( \frac{g_{*s}^0}{g_{*s}^{\text{d}}} \right)^{\frac{2}{3}}. \quad (43)$$

As the minimal free-streaming scale for  $\tau < t_{\text{eq}}$  it does depend on the the amount of dark radiation only. Referring to [61] to suppress scales of the size of a galaxy cluster  $v^0 \gtrsim 1$  km/s. In this case bounds at least similar to the HDM constraints seem to apply. For decays later than  $t_{\text{BBN}}$  we found a minimal velocity roughly three times larger and independent of the time of decay. If  $g_{*s}^{\text{d}} \sim 228.75 \gg g_{*s}^0$  the velocity is significantly

lowered but still too large to be compatible with Lyman- $\alpha$  limits. This confirms that the non-dominance bound is naive and indeed HDM constraints apply in any case.

### 2.3.2 Hot dark matter constraint and an opportunity

If a particle is relativistic at matter-radiation equality and became non-relativistic in the meantime, it represents hot dark matter (HDM). In particular, observations of the structure in the Universe constrain the amount of hot dark matter, which counts to  $\Omega_m$  but does not form structures below its large free streaming scale. Observations are used to derive upper bounds on the sum of the masses of the SM neutrinos  $\sum m_\nu$ . Bounds vary between 0.4 eV for the minimal model including large scale structure data and 2.6 eV if only CMB data is used and more parameters are included [62]. We re-write such bounds as constraints on the HDM fraction  $\Omega_{\text{hdm}}/\Omega_{\text{dm}} \leq b_{\text{max}}$ . It is

$$\begin{aligned} b_{\text{max}} &= \frac{\Omega_{\text{hdm}}^{\text{max}}}{\Omega_{\text{dm}}} = \left( \sum m_\nu \right)_{\text{max}} \frac{n_\nu^0}{\rho_c} \Omega_{\text{dm}}^{-1} \\ &= 0.098 \left( \sum m_\nu \right)_{\text{max}} / \text{eV}, \end{aligned} \quad (44)$$

where  $\Omega_{\text{dm}} \simeq 0.21$  has been inserted and  $n_\nu^0 = \frac{1}{11} N_\nu^{\text{SM}} n_\gamma^0$  is today's number density of one neutrino species, if  $n_\gamma^0$  denotes today's number density of CMB photons. We note that we have not taken into account the differing phase-space distributions of neutrino hot dark matter, described by a Fermi-Dirac distribution, and decay products with a phase-space distribution given by exponential decay in an expanding universe, see Appendix A. There are differences in the damping tails between decay produced dark matter and warm dark matter [60]. Nevertheless, given current measurement uncertainties and considering that constraints on HDM arise from observations on larger scales we assume the HDM bounds to apply unaltered.

As hot dark matter the corresponding decay product were non-relativistic today. Then its energy density  $\rho_2 = m_2 Y_2 s_0$ , when  $s_0$  denotes today's entropy density of the Universe and  $Y_2 = n_2/s$  the particle yield. Its yield is the same as the yield of the decaying particle if it did not decay,  $Y_2 = Y$ . Thus its energy density as hot dark matter today is just suppressed by the mass ratio of the two particles. It is

$$\Omega_2^{\text{hdm}} h^2 = \frac{m_2}{m} \Omega h^2 = \frac{\Omega h^2}{\delta + 1}, \quad (45)$$

where  $\Omega h^2$  is given by (19). Any constraint on the amount of hot dark matter simply yields an implicit lower bound on  $\delta$  as in (25) with only  $\Omega_{\text{dm}} \rightarrow \Omega_{\text{hdm}}^{\text{max}}$ . It is  $b_{\text{max}} < 1$  in (21) set by (44). For the bound depicted in Fig. 2 we choose a tight constraint, i.e.  $\sum m_\nu < 0.44$  eV at 95% CL [63] corresponding to  $b_{\text{max}} = 0.043$ , because this yields a strong lower bound on  $\delta$ . The temperature, when the heavier daughter becomes non-relativistic, corresponding to the obtained lower bound on  $\delta$  from hot dark matter constraints for  $\tau < (t_2^{\text{nr}})_{\text{min}}$ , i.e.  $T_2^{\text{nr}}(\delta = \delta_{\text{min}}^{\text{hdm}})$ , is obtained using (23) with  $b_{\text{max}}$  given by (44). We see that  $T_2^{\text{nr}}(\delta = \delta_{\text{min}}^{\text{hdm}})$  is lower than  $T_{\text{eq}}$ , which is to be expected. The bound appears self-consistent without further assumptions.

If  $\Delta N_{\text{eff}} > 0$  is observed, while observations exclude the heavier daughter becoming non-relativistic before a certain time, the actual lower bound on  $\delta$  would stem from the requirement of the heavier daughter to become non-relativistic after this late time, for example, the time of photon decoupling. This possible constraint is depicted in Fig. 2 as well.

We point out an interesting fact that leads to an opportunity. The neutrino mass scale sets two in principle independent quantities. These are: i) the neutrino energy density after they became non-relativistic,  $\Omega_\nu \simeq \sum m_\nu n_\nu$ , and ii) the time neutrinos become non-relativistic. The CMB alone is not very much affected, if the neutrinos are still relativistic at the time of photon decoupling, cf. Sec. 6.1 in [64]. As the thermal origin and thus the neutrino temperature is understood, this restricts the CMB sensitivity to masses  $m_\nu \gtrsim 0.6$  eV. The origin of HDM from a particle decay is very different. At what time the daughter becomes non-relativistic (8) depends on its mass only indirectly. The dependence is on the mass hierarchy to its mother as given by (45). Interestingly, a heavier daughter with an energy density above the tight HDM boundary from a decay with  $\tau \ll t_{\text{eq}}$  becomes non-relativistic at a time before photons finally decouple,  $t_2^{\text{nr}} < t_\gamma^{\text{dpl}}$ . In this case we expect the CMB to be sensitive to the heavier daughter acting as HDM. Such an amount of relativistic energy becoming non-relativistic during CMB times should leave observable consequences in the CMB even though the observational situation is not clear anymore. For sure, observations on smaller scales are affected.

By considering galaxy cluster data corresponding to a 10 Mpc scale  $N_{\text{eff}} = 3.91 \pm 0.42$  and  $\sum m_\nu = 0.34 \pm 0.17$  eV (both 95% CL) have been measured in [48] assuming free  $N_{\text{eff}}$  and  $\sum m_\nu$ . This is even not at 2- $\sigma$  non-zero, but the maximum likelihood constraint is peaked away from zero. Improvements to this analysis are said to be already approved. The obtained mean value might well be the first hint of the neutrino mass scale, while the largest mass-squared splitting from neutrino data is  $\sqrt{|\Delta m_{31}^2|} \simeq 0.050$  eV [65]. In Fig. 2 the required  $\delta$  to have  $\Delta N_{\text{eff}} = 0.86$  from the lighter daughter and  $\Omega_{\text{hdm}} = 0.004$  corresponding to  $\sum m_\nu = 0.34$  eV from the heavier daughter corresponds exactly to the upper edge of the thick solid black curve. Planck data combined with LSST or JDEM can constrain  $\sum m_\nu < 0.04$  eV [66, 67]. Experiments like KATRIN [68] or those seeking the neutrinoless double beta decay [69, 70] will measure neutrino masses in the laboratory. We point out an interesting possibility given these future sensitivities. If laboratory experiments measure  $m_\nu$  smaller than cosmological probes, this mismatch can be explained by a cosmological particle decay. The hot dark matter contribution in the Universe could have originated from particle decay. As we have shown the hot dark matter and dark radiation can originate from the same decay. Since the connection between observed mass scale and the time, when the HDM becomes non-relativistic, is different than for an additional relativistic species, these two cases should be distinguishable by future cosmological observations.

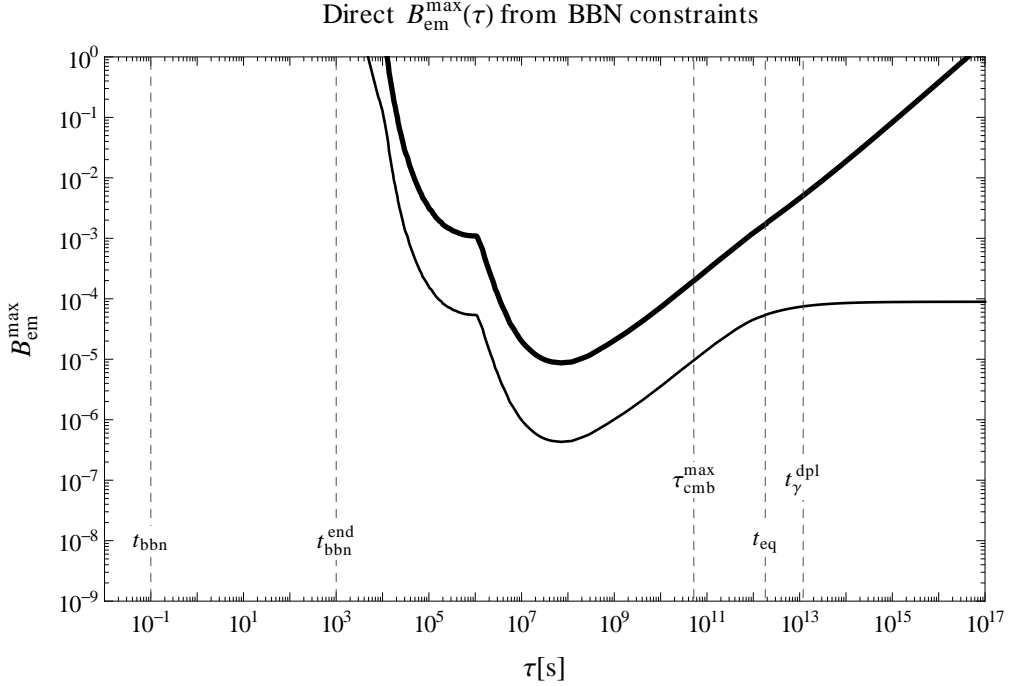


Figure 4: Upper bound from BBN on the direct branching ratio of the decaying particle into electromagnetically interacting particles as function of its lifetime  $\tau$ . The thick solid curve represents the weakest bound obtainable. We consider larger branching ratios as excluded. The thin solid curve represents the strongest bound obtainable. It shows how strong the actual bound might become depending on the actual value of  $\Delta N_{\text{eff}}$  and the energy density of the decaying particle after  $t_{\text{eq}}$ . Times are highlighted as in Fig. 2.

### 3 Branching ratio constraints and opportunities

In this section we derive constraints on several branching ratios of the decaying particle. Since the energy density of the decaying particle (19) is practically fixed for any significant value  $\Delta N_{\text{eff}} > 0$ , these bounds are general and, in particular, independent of the particle physics model.

**Bounds from BBN** We adopt the bounds from big bang nucleosynthesis (BBN) constraints determined in [71]. There the direct decay of some hypothetical massive particle into pairs of Standard Model particles,  $X \rightarrow \text{SM} + \text{SM}$ , is assumed. The product  $\Omega \times B_{\text{had/em}}$  is bounded, when  $B$  denotes the branching ratio into either hadronically (had) or electromagnetically (em) interacting pairs of Standard Model particles. Electromagnetic primaries are, for example, photons,  $\gamma\gamma$ , and electron-positron pairs,  $e^+e^-$ . Hadronic primaries are quarks,  $q\bar{q}$ , and gluons,  $gg$ . Hadronic decays generically lead to the injection of electromagnetically interacting primaries, for example, due to neutral pions decaying into two photons. The upper bound on corresponding branching ratios

is simply found as

$$B_{\text{had/em}}^{\text{max}} = \frac{\Omega_{\text{had/em}}^{\text{max}}}{\Omega}, \quad (46)$$

where  $\Omega_{\text{had/em}}^{\text{max}}$  is extracted from [71] and  $\Omega$  is given by (19). We will argue that the bounds are indeed independent of the kind of coupling and the existence of only one dark decay mode. For example, they do not depend on  $\delta$ , because  $\delta$  is in any case bounded from below by some cosmological requirement. So they might depend on this cosmological bound but not on the particle physics parameters.

Bounds from BBN depend on the cosmic time. The desired energy density of the decaying particle depends on the time of decay as well. Therefore, the resulting bounds are characteristic functions of the lifetime of the decaying particle. They are unique for the production of cosmic dark radiation. Upper bounds from BBN on the direct branching ratio into electromagnetically interacting particles are depicted in Fig. 4. Since they arise from the destruction of formerly build nuclei by, for example, photofission, they become effective at rather late times  $\sim 10^4$  s. However, they become severe with the strongest bound,  $B_{\text{em}}^{\text{max}} \sim 10^{-5}$ , around  $10^8$  s. Afterwards the bound becomes weaker as the energy density of the decaying particle decreases following (18). Bounds are provided in [71] up to  $10^{12}$  s. Towards later times we perform a trivial linear extrapolation. Such an extrapolation is crude, but we will see that CMB constraints are anyway stronger in this regime. Since no  $\Delta N_{\text{eff}} > 0$  is confirmed, we have to consider a range of possible values. A minimal value  $\Delta N_{\text{eff}}^{\text{min}} = 0.52$  might be set by the expected 2- $\sigma$  exclusion limit of Planck [19, 20]. As maximal value we take the 5- $\sigma$  exclusion of the combined analysis in [6]. It is  $\Delta N_{\text{eff}}^{\text{max}} = 5.265$ . These two different values lead to the spread of the two curves in Fig. 4 before the time of matter-radiation equality  $t_{\text{eq}}$ . This is the same for the solid and dashed curves in Fig. 5. The different behaviour after matter-radiation equality in both figures stems from the following: Before  $t_{\text{eq}}$  the conversion factor (17) is always nearly  $\mu$ , because  $\delta$  must be larger than  $\delta_{\text{min}}$  given by (27). Here, we implemented the bound from the non-dominance requirement, because smaller  $\delta$  results at later times in a stronger strong bound. After  $t_{\text{eq}}$  the maximal  $\Omega$  is given by  $\Omega_{\text{dm}}$  and  $\delta_{\text{min}}$  becomes smaller than one, which leads to the plateau of the strong bound after  $t_{\text{eq}}$ . For the weakest bound obtainable the conversion factor (17) is  $\mu$  also after  $t_{\text{eq}}$ , because  $\delta$  can also be arbitrarily large, if  $\Omega \simeq \Omega_{\text{rad}}$  instead. Thus the weak bound becomes weaker as  $\rho_{\text{rad}}$  decreases relative to  $\rho_{\text{mat}}$  due to the expansion of the Universe.

Upper bounds from BBN on the direct branching ratio into hadronically interacting particles are depicted in Fig. 5. They arise from different processes at different times. Charged mesons and antinucleons affect relic abundances already at times as early as  $\sim 10^{-1}$  s. Therefore, the hadronic branching ratio is bounded,  $B_{\text{had}}^{\text{max}} \sim 10^{-4}$ – $10^{-6}$ , already at such early times. The bound is strongest,  $B_{\text{had}}^{\text{max}} \sim 10^{-6}$ – $10^{-9}$ , around  $10^4$  s and afterwards becomes weaker, because the energy density of the decaying particle decreases. In determining the hadronic constraints we encounter specific additional uncertainties: First, it has been shown in [71] that the hadronic BBN bounds depend not only on the time of decay, but also on the actual value of the hadronic branching ratio. We find that this dependence is too weak to be important for our purpose.

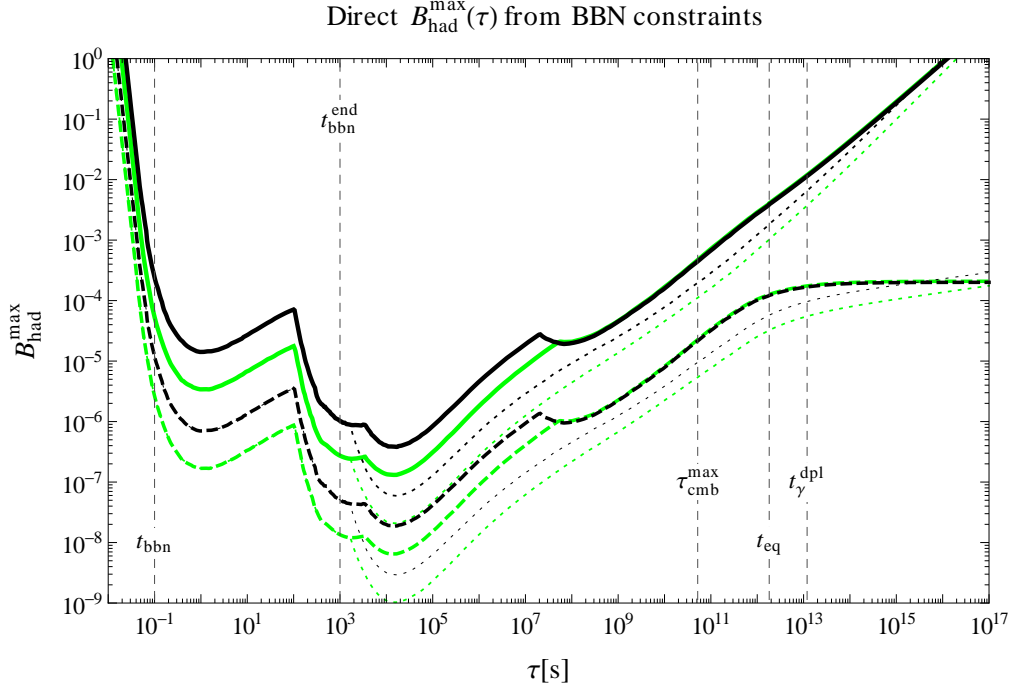


Figure 5: Upper bound from BBN on the direct branching ratio of the decaying particle into hadronically interacting particles as function of its lifetime  $\tau$ . Solid/dashed curves represent weakest/strongest bounds obtainable as in Fig. 4. Black curves apply to a mass of the decaying particle  $m = 1$  TeV and grey (green) curves to  $m = 100$  GeV. The thin dotted curves correspond in each case to a less conservative bound for the  ${}^6\text{Li}/{}^7\text{Li}$  ratio. Within the enclosed area the cosmic lithium problems could be solved by the decay. Times are highlighted as in Fig. 2.

Therefore, we assume a pure scaling of the bounds with the branching ratio between the extremal cases  $B_{\text{had}} = 1$  and  $B_{\text{had}} = 0$ . Second, the bound on the hadronic branching ratio has also been shown to depend on the mass of the decaying particle. If the mass is varied while the energy density is kept fix, the number density varies accordingly. To first order different effects cancel out. Bounds for two different masses of the decaying particle are provided to indicate the remaining dependence. Black curves in Fig. 5 apply to a mass of the decaying particle  $m = 1$  TeV and grey (green) curves to  $m = 100$  GeV. Referring to Fig. 10 we note that it might be motivated by the production of dark radiation from particle decay to extend an analysis of BBN constraints towards smaller masses,  $m < 100$  GeV, of the decaying particle. Third, the determinations of  ${}^6\text{Li}$  and  ${}^7\text{Li}$  abundances are affected by uncertainties in the understanding of nuclei destruction processes in stars. The thin dotted curves in Fig. 5 correspond in each case to a less conservative bound for the  ${}^6\text{Li}/{}^7\text{Li}$  ratio. Branching ratios above these curves but below the corresponding more conservative bounds should not be regarded as ruled out.

In contrast, if they do not violate other bounds, they are a possible explanation for the

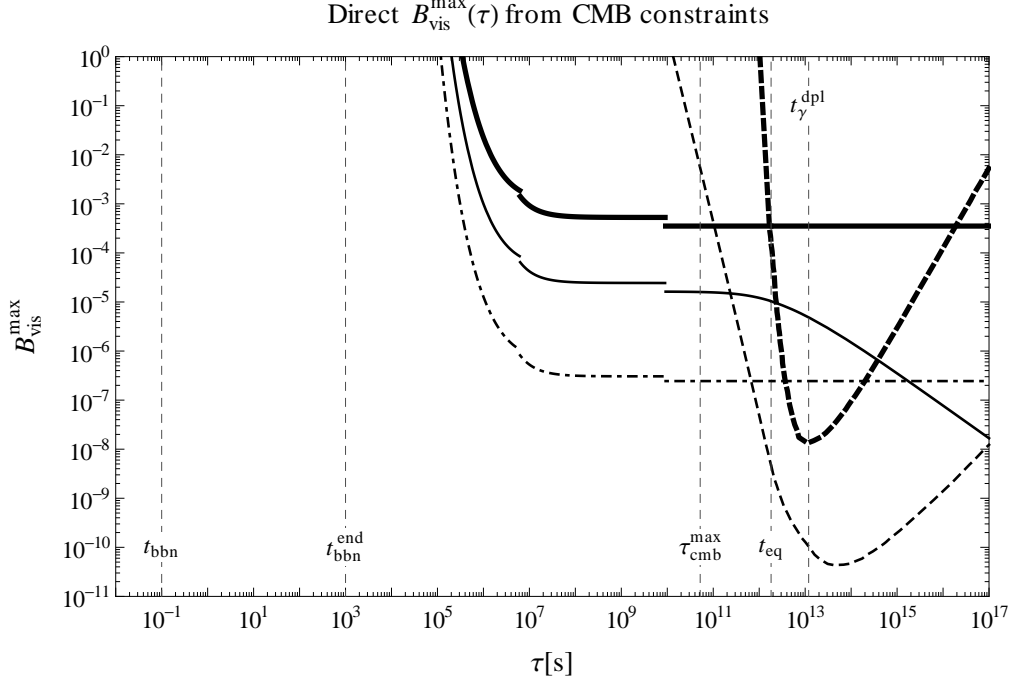


Figure 6: Upper bound from the CMB on the direct branching ratio of the decaying particle into photons and electron-positron pairs as function of its lifetime  $\tau$ . Thick/thin solid curves represent weakest/strongest bounds obtainable as in Fig. 4 from spectral distortions on the branching ratio into photons  $B_\gamma$ . In the same sense thick/thin dashed curves represent weakest/strongest bounds obtainable from the ionisation history on the branching ratio into electrons, positrons and/or photons. The dash-dotted curve indicates PIXIE’s discovery reach, if  $\Delta N_{\text{eff}} = 1$ ,  $Y_p = 0.249$  and  $g_{\text{dr}}^{\text{obs}} = 2$ . Times are highlighted as in Fig. 2.

relatively high  ${}^6\text{Li}/\text{H}$  ratios observed in metal-poor halo stars providing the cosmic origin of  ${}^6\text{Li}$  [45]. If the observationally inferred  ${}^7\text{Li}/\text{H}$  ratio is solved by stellar depletion, both problems, known as the cosmic lithium problems could be solved by the same particle decay. At this point it is important to remind that the bounds in Fig. 4 apply equally to hadronic primaries, because they inject numerous electromagnetic primaries. These are also constrained in the following section.

**Bounds from CMB** The emission of particles with Standard Model interactions leads to spectral distortions of the cosmic microwave background (CMB). As in the previous section, we exploit the fact that the energy density of the decaying particle is fixed by the amount of dark radiation. To determine an upper bound on the branching ratio into photons we update the analysis of [72] by taking into account the corrections pointed out in [73] and the current limits on deviations of the CMB from a thermal spectrum. These, obtained by COBE FIRAS, are  $|\mu| < 9 \times 10^{-5}$  and  $y < 1.5 \times 10^{-5}$  [74, 75]. We



find

$$B_\gamma \lesssim 0.66 \mu_{\max} \Delta N_{\text{eff}}^{-1} g_{\text{dr}}^{\text{obs}} (g_*^{\text{d}})^{\frac{5}{4}} e^{(t_\mu/\tau)^{\frac{5}{4}}}, \quad (47)$$

where  $\mu_{\max}$  denotes the bound on  $\mu$  and  $t_\mu \simeq 6.91 \times 10^6 \text{ s} (1 - Y_p/2)^{4/5}$  the timescale of thermalization in the Universe at that epoch. It is set by the primordial helium abundance  $Y_p$  and other cosmological parameters, where we inserted PDG mean values [51]. Following [73] we replace  $e^{(t_\mu/\tau)^{5/4}} \rightarrow 0.48(\tau/t_\mu)^{10/18} e^{1.99(t_\mu/\tau)^{10/18}}$  for times earlier than  $t_\mu$ . Upper bounds on the direct branching ratio into photons  $B_\gamma$  from spectral distortions of the CMB are depicted as solid curves in Fig. 6. They are not effective at times earlier than  $3 \times 10^5 \text{ s}$ , because injected photons thermalise safely not leaving any observable imprint. In the analytic approximation (47) this is explicated by the exponential factor. For  $\tau \gtrsim t_\mu$  the weak bound becomes constant on a severe level,  $B_\gamma^{\max} \simeq 4 \times 10^{-4}$  or  $2 \times 10^{-5}$ . This is a qualitative difference to the BBN bounds. At a certain time around  $2 \times 10^{11} \text{ s}$  they become stronger than the bounds in Fig. 4. Therefore, the extrapolation of the BBN bounds towards later times is not crucial for our purpose. The spread between the strongest bounds obtainable (thin curves) and the weakest bounds obtainable (thick curves) is mainly due to the same reasons as for the bounds from BBN on the electromagnetic branching ratio depicted in Fig. 4. To consider the relatively large observational uncertainty in the primordial  ${}^4\text{He}$  abundance we take for the strong bound  $Y_p = 0.267$  and for the weak one  $Y_p = 0.231$ , which corresponds to the  $2\text{-}\sigma$  statistical and systematic PDG error range [51]. No change of slope arises at  $t_{\text{eq}}$  from the change in the expansion law, because it turns out that in our parametrisation the bound function (47) has no proportionality to the time of decay. For times  $\tau \lesssim 4 \Omega_b h^2 \times 10^{11} \text{ s}$  elastic Compton scattering establishes a Bose-Einstein spectrum with chemical potential  $\mu$  regardless of the details of the injection. For the considered case of massive particle decay, the number of injected photons is negligible relative to the number of photons in the background. In any case the energy density of injected photons has to be small compared to the energy density of background photons. Then the induced chemical potential is proportional to the injected energy density,  $\mu \propto B_\gamma \rho / \rho_\gamma$ . For times  $\tau \gtrsim 4 \Omega_b h^2 \times 10^{11} \text{ s}$  the spectrum can be described by the Compton  $y$ -parameter. The jump in the bound due to this change in the description of the spectrum with the corresponding constraints is easily identified in Fig. 6 around  $10^{10} \text{ s}$ . It is  $B_\gamma \rho / \rho_\gamma = 4y$ .

Future CMB polarimeters such as PIXIE are proposed providing dramatically tighter constraints with projected detection levels of  $\mu \sim 5 \times 10^{-8}$  and  $y \sim 10^{-8}$  at  $5\text{-}\sigma$  [76]. The dash-dotted curve indicates PIXIE's discovery reach, if  $\Delta N_{\text{eff}} = 1$ ,  $Y_p = 0.249$  and  $g_{\text{dr}}^{\text{obs}} = 2$ . PIXIE could even identify the origin of a spectral distortion as particle decay [73, 77]. Comparing Fig. 6 and 9 with the corresponding hadronic bounds we see that due to the specific behaviour of the bounds large portions of parameter space probed by PIXIE are neither excluded by BBN nor by changing the ionisation history of the Universe.

The emission of particles with Standard Model interactions may change the ionisation history of the Universe, which can leave observable consequences in the CMB. We adopt the bounds on scenarios with late-decaying particles derived in [78] based upon WMAP7 limits. Upper bounds on the direct branching ratio into electron-positron pairs



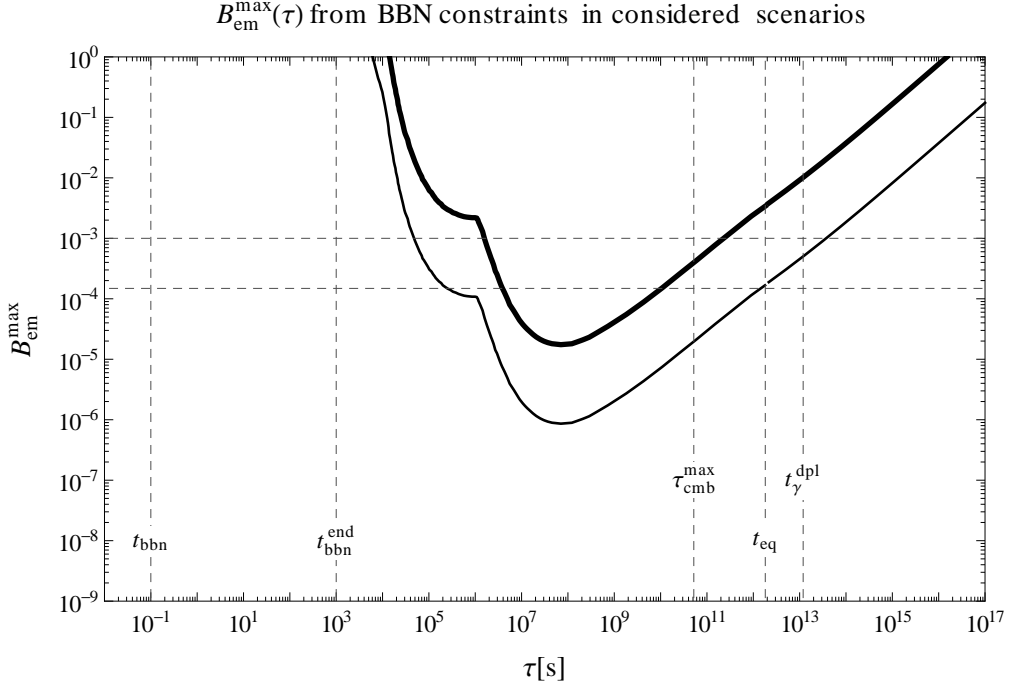


Figure 7: As Fig. 4 but on the off-shell or non-tree-level branching ratio of the decaying particle as applying to the scenarios under consideration. Horizontal lines indicate i) the often quoted suppression of  $10^{-3}$  for off-shell processes and ii) the suppression from an electromagnetic loop and three-to-two-body kinematics.

or photons from additional ionisation and heating observable in the CMB are depicted as dashed curves in Fig. 6. They become effective at a much later time around  $\tau_{\text{cmb}}^{\text{max}}$  and  $t_{\text{eq}}$ , but also quickly stronger than the bounds from spectral distortions. They are strongest already around  $t_{\gamma}^{\text{dpl}}$  and then become weaker towards later times as the energy density of the decaying particle decreases and a decay has less impact on observables. Nevertheless, they stay strong till today, in particular, stronger than bounds from spectral distortions at late times. In [78] for each lifetime it is scanned over the constraint for photons and electron-positron pairs for masses of the decaying particle ranging from 2 keV to 12 TeV. The bound becomes a band with its width reflecting the variation in the bound between different decaying particle masses and decay products. To consider this uncertainty we take the strongest bound provided for our strong bound and the weakest bound provided for our weak bound, respectively. This approach is sufficient for our purpose, because the weakest bound obtainable from spectral distortions is already quite strong. Nevertheless, we would like to point out that this uncertainty –for example, 1.1 orders of magnitude at  $\tau = 10^{14}$  s– could be reduced to a negligible level referring to [78]. Since we provide the injection spectrum and the variation with redshift, one should be able to do so using the provided grid of injection energies and redshifts. Referring to Fig. 10 we note that it might be motivated by the production of

dark radiation from particle decay to extend the analysis of these constraints towards smaller masses,  $m < 1$  keV, of the decaying particle.

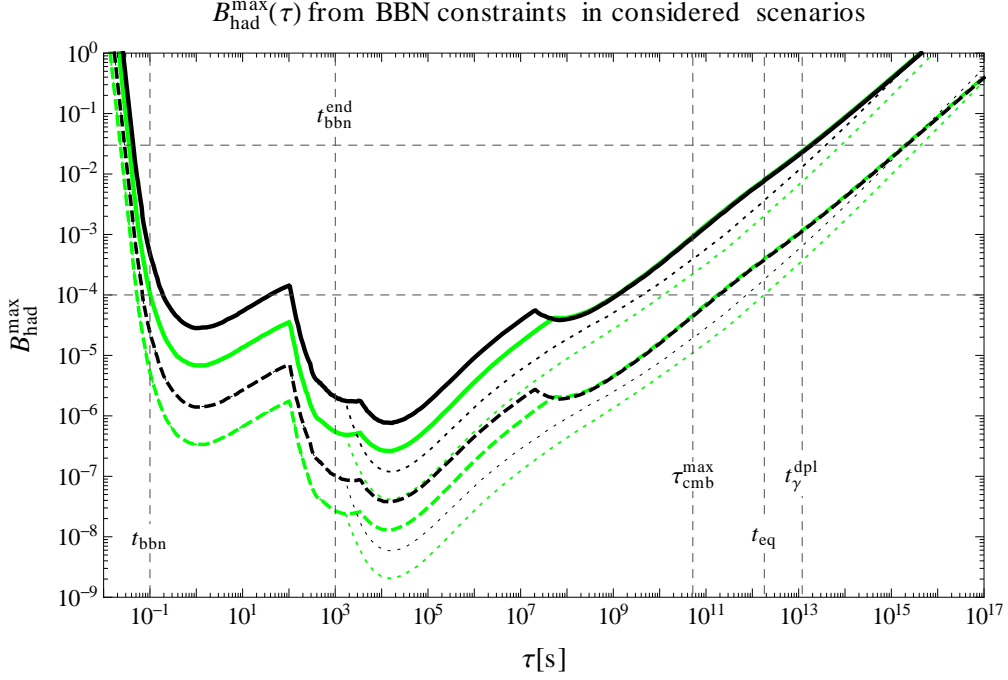


Figure 8: As Fig. 5 but on the off-shell or non-tree-level branching ratio of the decaying particle as applying to the scenarios under consideration. Horizontal dashed lines indicate: i) the minimal hadronic branching ratio  $\simeq 0.03$  of a neutralino decay into gravitino calculated in [79] and ii) the minimal hadronic branching ratio  $\sim 10^{-4}$  of a sneutrino decay into gravitino for sneutrino masses  $\gtrsim 200$  GeV and  $\delta > 9$  found in [80].

**Bounds on considered scenarios** In the previous paragraphs we determined cosmological constraints on the direct decay,  $X \rightarrow \text{SM} + \text{SM}$ , into various decay products with Standard Model interactions. As discussed these bounds are severe and any model must satisfy them. For the scenarios considered in this work we assume that this is the case. In Sec. 2 we consider models without any tree-level decay mode that could give rise to a constrained branching ratio. This means that the constrained direct branching ratios are automatically zero. If, for example, photons are emitted on tree-level, the decay would have to occur before  $\tau \lesssim 10^4$  s and so on. Thus all these constraints are fulfilled by construction. Dangerous summands in the Lagrangian are forbidden kinematics or by symmetries, which is relatively simple. This either holds true for the models under consideration in Sec. 4 or dangerous tree-level modes are sufficiently suppressed. We repeat that this often means branching ratios smaller than  $10^{-4}$ . While tree-level branching ratios arise in a relatively simple way from the theory, higher order corrections contain further information about the theory. In any case de-

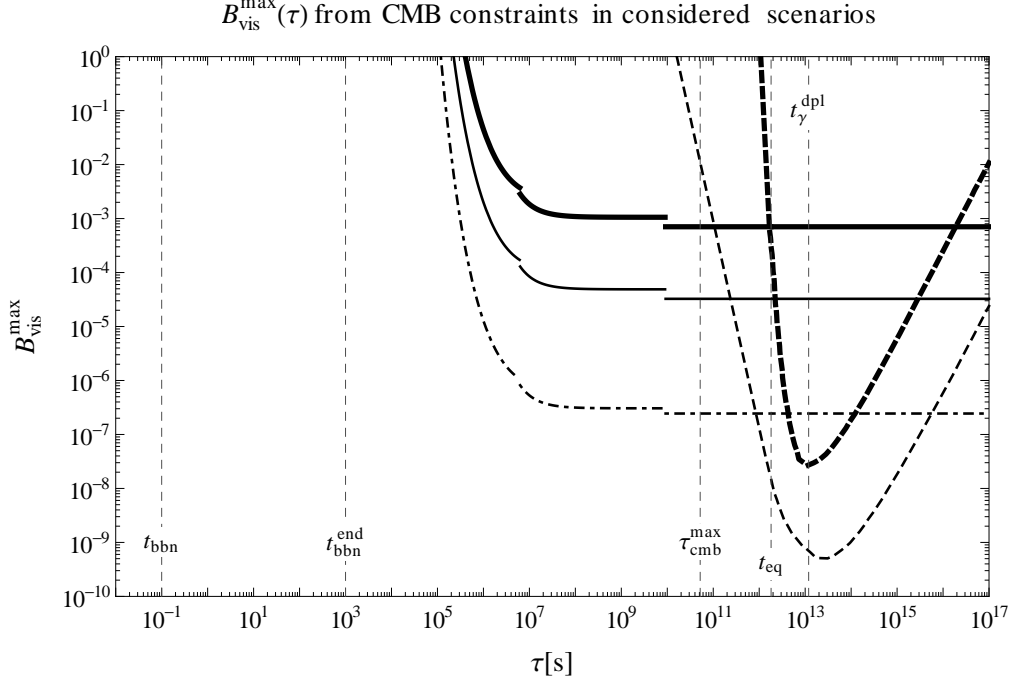


Figure 9: As Fig. 6 but on the off-shell or non-tree-level branching ratio of the decaying particle as applying to the scenarios under consideration.

cays emitting particles with SM interactions may proceed off-shell or via loop processes,  $X \rightarrow \text{dark} + ?^* \rightarrow \text{dark} + \text{SM} + \text{SM}$ . Then the previously given bounds do not apply. Three-body final states might yield the leading contribution. Shortened, we have to consider how much energy is carried away invisibly in each decay.

At early decay times,  $\tau \ll t_{\text{eq}}$ , the situation is very simple. Half of the energy will always be carried away by some dark decay product as we found already that both have to be emitted relativistically with equal momenta. The case that both decay products go off-shell or couple in a loop can safely be neglected, because the matrix element is additionally suppressed and leads to four-body final states. These are also suppressed kinematically. At later decay times,  $\tau > t_{\text{eq}}$ , heavier decay products might be emitted non-relativistically. Actually, this is by construction the case for the strong bounds depicted in Figs. 4, 5 and 6. The virtuality of particles with  $p < m$  is small. It is very improbable that they decay off-shell or even couple in a loop. Therefore, it is a very good approximation to assume them to be safe. Only the decay products forming the dark radiation or –at least– being emitted relativistically are left to endanger observations in this case. Altogether, to determine upper bounds on the off-shell or non-tree-level branching ratio of the decaying particle we multiply (19) by  $((\delta + 1)^2 - 1)/(2(\delta + 1)^2)$ . This is to consider the amount of energy which is always carried away invisibly. The second factor cancels the dependence on  $\delta$  in (19). Actually, this factor is universal in the sense of quantifying the relativistically emitted fraction of energy as we found that

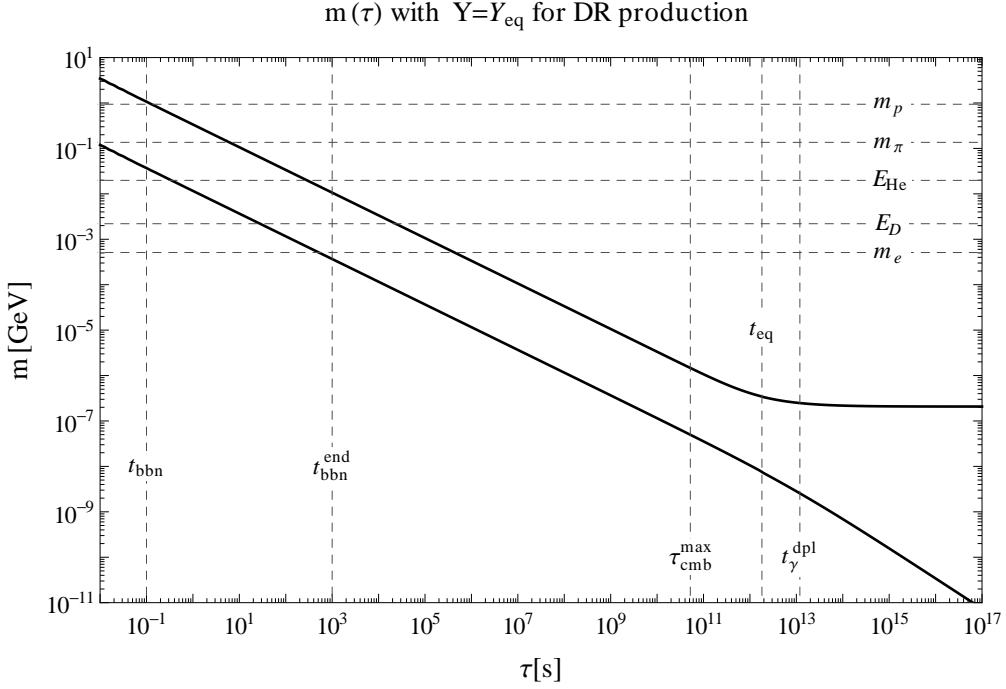


Figure 10: Allowed masses  $m$  for a decaying particle with large equilibrium yield. Within the lower ( $mY = (mY)_{\min}$ ,  $Y_{\text{eq}}(g_* = g_*^{\text{SM}} = 106.75)$ ) and upper ( $mY = (mY)_{\max}$ ,  $Y_{\text{eq}}(g_* = 228.75)$ ) line a decaying particle, which left thermal equilibrium being relativistic at some early time, might produce the desired amount of dark radiation depending on  $g_*$  and the type of particle. Horizontal lines indicate masses of the proton  $m_p$ , the pion  $m_\pi$ , the electron  $m_e$  and photodissociation thresholds of  $^4\text{He}$  and deuterium, respectively. Times are highlighted as in Fig. 2.

$\delta$  is not free, but has to satisfy bounds. Applied to the scenarios of Sec. 4 this means  $B_{\text{dr}} = B_1 \stackrel{!}{=} \frac{(\delta_{\min}+1)^2-1}{(\delta_{\min}+1)^2}$ , while the situation is odd, because it is restricted to an odd window of mass hierarchies,  $1/4 < x_2 < 1/2$ , see Sec. 4. The resulting bounds are depicted in Fig. 7, 8 and 9 analogously to Fig. 4, 5 and 6. Compared to those on direct branching ratios all bounds are reduced by  $1/2$ . More importantly, there is no additional spread between strong and weak bound after  $t_{\text{eq}}$  for off-shell and non-tree-level branching ratios.

The obtained bounds are severe and have the power to exclude many particle physics possibilities. As demonstration we give two examples: i) From Fig. 4 a neutralino LOSP could decay during or even after BBN,  $\tau \lesssim 10^4$  s, into a gravitino and a photon. The photon thermalises safely and the gravitino could act as dark radiation. However, as shown in Fig. 8 this is excluded for  $4 \times 10^{-2}$  s  $\lesssim \tau \lesssim t_\gamma^{\text{dpl}}$  due to the minimal hadronic branching ratio of this decay. It arises from the off-shell decay of the massless photon into  $q\bar{q}$  pairs enhanced by a logarithmic infrared divergence, see [79] for details. It is thus too large even for neutralino masses as small as some tens of GeV. ii) A sneutrino

LOSP can decay invisibly into a gravitino and a neutrino both possibly acting as dark radiation. The bounds in Fig. 4, 5 and 6 are evaded. However, the weak interactions of the sneutrino and the neutrino lead to a hadronic branching ratio with significant impact on BBN, if the sneutrino is sufficiently heavier than the electroweak gauge bosons. The minimal branching ratio of  $\sim 10^{-4}$  for sneutrino masses  $\gtrsim 200$  GeV and  $\delta > 9$  found in [80] is depicted in Fig. 8. We see that the decay is excluded for  $10^{-1} \text{ s} \lesssim \tau \lesssim 10^9 \text{ s}$ .

In Fig. 10 we show the band of allowed masses for a decaying particle, which entered thermal equilibrium and then decoupled being relativistic at some early time. Thus it has a relatively large yield. Larger yields can be reached in non-thermal production mechanisms. The figure serves to make an important point. We can see that for such yields the mass of the mother is restricted to be smaller than  $\sim 2$  GeV for decays occurring during or after BBN. For masses of the mother smaller than the proton mass no nuclei can be emitted. Thus no BBN constraints from the injection of nuclei apply. For masses of the mother smaller than the pion mass no hadronically interacting particles can be emitted at all and so on. Emitted photons with energies below photodissociation thresholds do not destroy corresponding nuclei. A small enough mass of the decaying particle can thus circumvent all BBN constraints. It might be motivated by the production of dark radiation from particle decay to extend analyses of BBN constraints towards masses smaller than 100 GeV. There should be non-trivial effects, when the mass of the mother approaches the proton mass and so on. Regarding the ionisation history of the Universe the effect of photons emitted with energies smaller than one keV seem worth to be studied.

## 4 Two dark decay modes

In this section we study the origin of dark radiation from the two-body decay of a non-relativistic particle, which possesses two dark decay modes with corresponding branching ratios  $B_{1,2}$  summing up to roughly one,

$$B(X \rightarrow 1 + 1) + B(X \rightarrow 2 + 2) = B_1 + B_2 \simeq 1, \quad (48)$$

where 1 and 2 denote and label the two dark decay products. It is shown in Sec. 3 that the branching ratio into dark components is constrained to be very close to one at times later than  $t_{\text{BBN}}$ . Considering the upper right corner of Fig. 1, there is no heavier/lighter daughter in each decay. In contrast, there are lighter daughters from one decay mode and heavier daughters from an additional decay mode. Compared to the cosmologies in Sec. 2 there is one additional parameter, the relative branching  $B_1/B_2$ . This allows for the dash-dotted curve in Fig. 1, where  $B_2$  is obviously much smaller than one.

Well-motivated examples for such decays are i) saxion decays into two axinos with  $y^2 \sim m_{\text{sax}}^2/(4f_a^2)$ , where  $m_{\text{sax}}$  denotes the saxion mass and  $f_a$  the axion decay constant, ii) moduli decays into two gravitinos with  $y^2 \sim \kappa^2 m_\phi^2/(18M_{\text{pl}}^2)$ , where  $m_\phi$  denotes the modulus mass and  $\kappa$  an effective coupling, iii) saxion decays into two axions with  $y^2 \sim x^2 m_{\text{sax}}^2/(4f_a^2)$ , iv) flaton decays into two axions with  $y^2 \sim m_f^2/(2f_a^2)$  [81], where  $m_f$  denotes the flaton mass or v) moduli decays into bulk axions with  $y^2 \sim m_\phi^2/(2M_{\text{pl}}^2)$  [32,

33]. In i)+ii) a scalar decays into two fermions, while in iii)-v) a scalar decays into two scalars. Other combinations of spins are imagineable. Note that in theories beyond the Standard Model with a dark matter stabilising symmetry either interactions as thought about here or in Sec. 2 may be allowed for the same particle. Depending on the number of long-lived particles in the theory there may be particles of each kind in the spectrum. As one might infer from the given lists, this is the case, for example, in supergravity theories amended by the Peccei-Quinn mechanism.

Even though all decay products may act as dark radiation, especially, the heavier ones do not need to do so at any time. In contrast, they may form the observed dark matter. Then two of three dark components originate from the same decay. This has been proposed first in [41], where the authors also take into account BBN constraints.

## 4.1 Basics

We introduce useful parameters, determine general properties and derive basic equations.

**Kinematics** In each decay the two decay products have equal mass, so that the general expression for the initial momentum (1) of each emitted particle reduces to

$$p_{\text{ini}} = p_{1,2} = \frac{m}{2} (1 - 4x_{1,2}^2)^{\frac{1}{2}} \quad (49)$$

with  $x_{1,2} = m_{1,2}/m$  denoting the mass ratio of the corresponding daughters with equal mass and the mother particle. This parameter is a useful measure of their mass hierarchy. We choose labels such that  $m_1 < m_2$ . It is always  $m_1, m_2 < m/2$  otherwise the corresponding decay were kinematically forbidden. Non-relativistic emission can occur only in the odd mass window  $m/4 < m_2 < m/2$ . This scenario might appear rather unattractive for model building from the naturalness point of view. The other way around, a theory predicting  $m_2$  in this range would interestingly always lead to this case.

**On  $T_{1,2}^{\text{nr}}$  and  $1/x$ - $\tau$  plane** From the same general condition (7) we find the temperature, when the corresponding daughters become non-relativistic,

$$T_{1,2}^{\text{nr}} = T_{\text{d}} \frac{2}{\mu} (x_{1,2}^{-2} - 4)^{-\frac{1}{2}} \left( \frac{g_{*s}^{\text{d}}}{g_{*s}^{\text{nr}}} \right)^{\frac{1}{3}} \quad (50)$$

with  $g_{*s}^{\text{nr}} = g_{*s}(T_{1,2}^{\text{nr}})$ . Typical requirements on  $T_{1,2}^{\text{nr}}$  might be that: i) the particle is still relativistic today,  $T_{1,2}^{\text{nr}} < T_0$ , which is the best –or only– understood situation from the observational point of view, ii) the particle does not become non-relativistic during CMB times,  $T_{1,2}^{\text{nr}} < T_{\gamma}^{\text{dpl}}$  or  $T_{1,2}^{\text{nr}} > T(\tau_{\text{cmb}}^{\text{max}})$ , which would possibly leave some observable signature in the CMB, or iii) the particle does or does not act as radiation at matter-radiation equality,  $T_{1,2}^{\text{nr}} < T_{\text{eq}}$  or  $T_{1,2}^{\text{nr}} > T_{\text{eq}}$ . Such requirements turn into constraints on

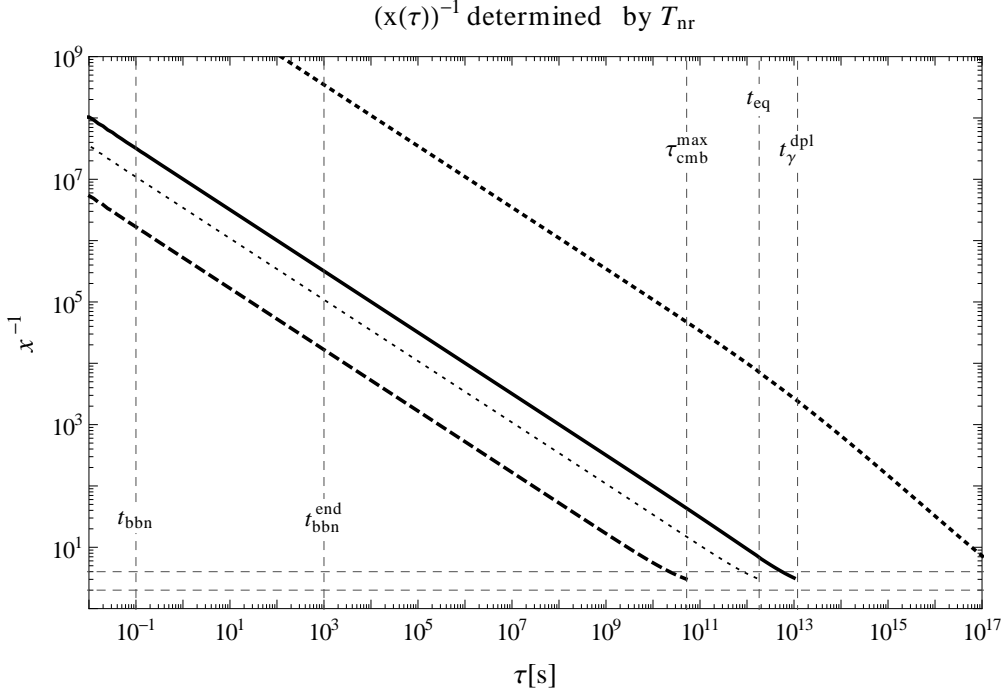


Figure 11: Mass hierarchy  $1/x_{1,2} = m/m_{1,2}$  given by (51) for different requirements on  $T_{1,2}^{\text{nr}}$ . On the solid curve the decay products become non-relativistic at the time of photon decoupling. For smaller values of  $x$  particles become non-relativistic at later times. In the same sense the dashed curve corresponds to  $t_{1,2}^{\text{nr}} = \tau_{\text{cmb}}^{\text{max}}$ , the thin dotted curve to  $t_{1,2}^{\text{nr}} = t_{\text{eq}}$  and for a decay product to be still relativistic today  $1/x_{1,2}$  would have to lie above the thick dotted curve. Within the horizontal dashed lines the corresponding decay product is emitted non-relativistically. Values of  $x > 1/2$  do not exist. Times are highlighted as in Fig. 2.

$x_{1,2}$  depending on the time of decay. From (50) it is straightforward to single out

$$x_{1,2} = \frac{1}{2} \left( \left( \frac{T_d}{T_{1,2}^{\text{nr}}} \right)^2 \frac{4}{\mu^2} \left( \frac{g_{*s}^d}{g_{*s}^{\text{nr}}} \right)^{\frac{2}{3}} + 4 \right)^{-\frac{1}{2}}. \quad (51)$$

The constraints on  $x_{1,2}$  from the requirements i)-iii) on  $T_{1,2}^{\text{nr}}$  are shown in Fig. 11.

**Energy densities** The desired amount of dark radiation determines the energy density of the decaying particle. In principle, both decay channels can contribute to an increase in  $\Delta N_{\text{eff}}$ , which might be interesting on its own only if both add some observable contribution so for  $B_1 \sim B_2$ . There is a plethora of possible cosmologies. For example, both can contribute dark radiation at BBN and/or photon decoupling. Heavier decay products could become non-relativistic in the meantime, while lighter ones are

still relativistic today, and so on. We shall focus on the case that the dark radiation at the time of observation is formed by the lighter daughters only,  $\rho_{\text{dr}} = \rho_1$ . Anyways the following holds analogously in and can be applied to other cases.

Since  $B_1 + B_2 \simeq 1$ , the number densities of the decay products at decay are given by

$$n_{1,2} \simeq 2nB_{1,2}. \quad (52)$$

If the dark radiation is formed by the lighter daughter particles,

$$\rho_{\text{dr}} = \rho_1 = n_1 E_1, \quad (53)$$

where  $E_1 \simeq \langle p_1 \rangle$ , because they must be relativistic to act as radiation. At the decay  $p_1$  is given by (49) and  $n_1$  by (52). In this way the energy density of the decaying particle  $\rho = nm$  at the decay is set by the amount of dark radiation. The mean  $\langle p_1 \rangle / p_{\text{ini}} = \mu$  is given by the distribution in Appendix A. It is

$$\rho|_{\text{dec}} = \mu^{-1} B_1^{-1} (1 - 4x_1^2)^{-\frac{1}{2}} \rho_{\text{dr}}(T_d), \quad (54)$$

where  $\rho_{\text{dr}}(T_d)$  has been found in (15). The previously defined conversion factor (17) would read in this case  $\mu B_1 (1 - 4x_1^2)^{1/2}$ .

After the heavier daughters became non-relativistic, their energy density,  $\rho_2 = n_2 E_2 \simeq n_2 m_2$ , can be related to the energy density of the mother, if it would not have decayed, by making use of the definition of  $x_2$  and inserting (52). It is  $\rho_2 = 2B_2 x_2 \rho$  or today

$$\Omega_2 h^2 = 2B_2 x_2 \Omega h^2 = 2B_2 x_2 \left( \frac{T_0}{T_d} \right)^3 \frac{g_{*s}^0}{g_{*s}^d} \frac{\rho|_{\text{dec}}}{\rho_c}, \quad (55)$$

where the energy density at decay is fixed by (54). Note that this is valid for times only, when the heavier daughters are non-relativistic.

## 4.2 Non-dominance requirement and dark matter

The non-dominance requirement, cp. (21), on the heavier daughters gives by (55) rise to an upper bound

$$\frac{x_2}{B_2^{-1} - 1} \leq 2.626 \times 10^{-3} \mu \left( \frac{1 \text{ keV}}{T_d} \right) \left( \frac{g_{*s}^0}{g_{*s}^d} \right)^{\frac{1}{3}} \Delta N_{\text{eff}}^{-1} \left( \frac{\Omega_{\text{dm}} h^2}{0.1246} \right) (1 - 4x_1^2)^{\frac{1}{2}}, \quad (56)$$

where we used further that  $B_{1,2}$  are no independent parameters but linked by the definition of the scenario (48). In particular,  $B_2/B_1 = 1/(B_2^{-1} - 1)$ . If then  $x_2$  or  $B_2$  are fixed by the particle physics model, the other of the two became fix making use of (56). For  $\tau > t_{\text{eq}}$  the heavier daughters are either emitted relativistically as the lighter ones or their mass were restricted to the odd window  $m/4 < m_2 < m/2$ . For  $\tau < t_{\text{eq}}$  the requirement simplifies, because: i)  $x_1$  is much smaller than one, cp. Fig. 11, and ii)  $B_2$



will be typically much smaller than one for the heavier daughter to make up a viable dark matter candidate, so that  $(B_2^{-1} - 1)^{-1} \simeq B_2$ . Then (56) reduces to

$$B_2 x_2 \lesssim 6.415 \times 10^{-3} \left( \frac{\tau}{10^7 \text{ s}} \right)^{\frac{1}{2}} \Delta N_{\text{eff}}^{-1} \left( \frac{\Omega_{\text{dm}} h^2}{0.1246} \right) \left( \frac{g_*^{\text{d}}}{g_*^0} \right)^{\frac{1}{4}} \left( \frac{g_{*s}^0}{g_{*s}^{\text{d}}} \right)^{\frac{1}{3}}. \quad (57)$$

A theory linking  $B_2 x_2$ , such that this non-trivial constraint is fulfilled naturally, appears particularly attractive.

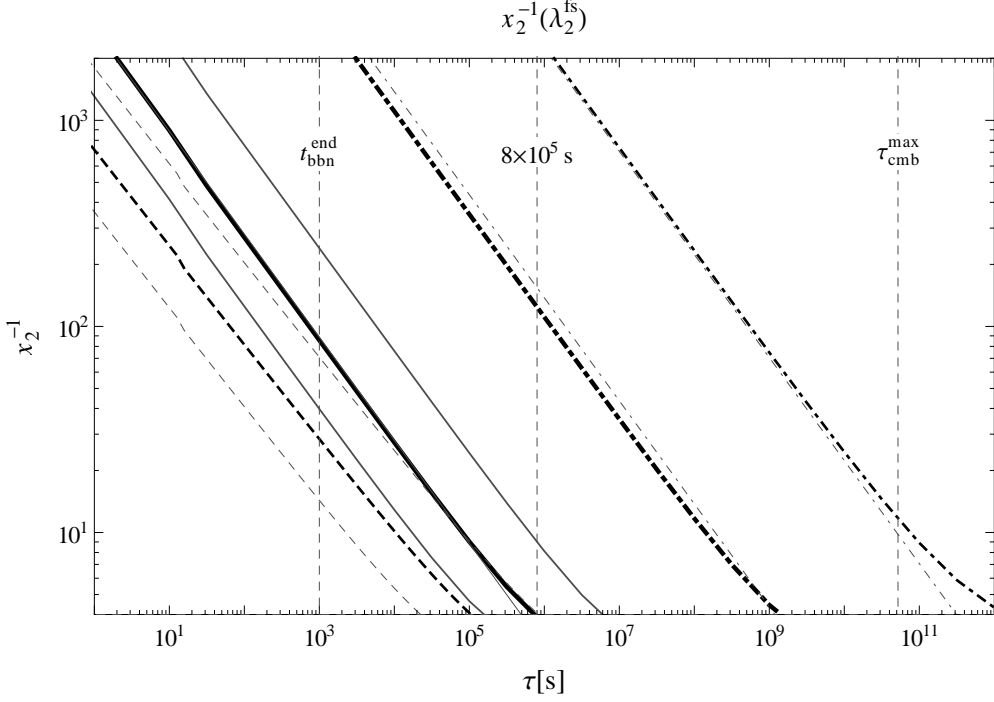


Figure 12: The required  $x_2 = m_2/m$  depending on the time of decay to obtain a certain free-streaming scale  $\lambda_2^{\text{fs}}$ . The thick solid curve corresponds to the numerical solution of (58) for  $\lambda_2^{\text{fs}} = 0.4$  Mpc. The area with  $0.2 \text{ Mpc} \leq \lambda_2^{\text{fs}} \leq 1 \text{ Mpc}$  is found within the thin solid curves. Values above the upper thin curve are excluded if the heavier daughter is to form the observed dark matter. Values below the lower thin curve do not leave an observable imprint in the sky. The heavier daughters form cold dark matter in this area, if  $B_2$  satisfies (56) at the boundary. The dashed curves provide the same information for the analytic estimate (60). Above the thick dash-dotted curve  $\lambda_2^{\text{fs}} > 10$  Mpc. The thin dash-dotted curve corresponds to  $\lambda_2^{\text{fs}} = 100$  Mpc and is given for better orientation. Overplotted as very thin grey curve is the simple analytic approximation (59). Barely visible for  $\lambda_2^{\text{fs}} = 4$  Mpc it is slightly too small for 10 Mpc, while the fit for 100 Mpc is almost perfect again. We can read off that in a decay after  $8 \times 10^5 \text{ s}$  the decay products have to be emitted non-relativistically to obtain  $\lambda_{\text{fs}} = 0.4$  Mpc, because the required  $x_2$  becomes smaller than  $1/4$ . Other times are highlighted as in Fig. 2.

In principle after being emitted also the heavier decay products may act as dark radiation throughout the history of the Universe. However, they do not need to act as radiation at any time. At the boundary the heavier daughters form the observed dark matter,  $\Omega_2 = \Omega_{\text{dm}}$ , which energy density depends on the energy density of dark radiation as explicated in Sec. 2.3. We find that they can, indeed, form the observed dark matter. We will see how structure formation provides additional constraints on  $B_2$  and  $x_2$ . To act as cold dark matter, for example,  $x_2$  must lie below the thin solid curve in Fig. 12. If this bound is violated, tighter constraints than (56) apply. For example, if they act as hot dark matter, we must replace  $\Omega_{\text{dm}} \rightarrow \Omega_{\text{hdm}}^{\text{max}}$ . Since the free-streaming scale of the heavier daughters is set and can be adjusted by the involved couplings and masses, there are not only constraints but opportunities arising from the heavier daughters in structure formation.

### 4.3 Solution to the missing satellites problem

In simulated cold dark matter halos there is an overabundance of substructures with respect to the observed number of Milky Way satellites [46, 47] known as the missing satellites problem. The dispersion of structure on these small scales reduces the predicted number of galactic satellites. In particular, warm dark matter with a free-streaming scale  $\lambda_{\text{fs}} \gtrsim 0.2$  Mpc resolves the missing satellites problem [82, 83, 84]. We mentioned above the upper bound  $\lambda_{\text{fs}} \lesssim 1$  Mpc from Lyman- $\alpha$  forest data. In [85] the authors considered the late decay of a massive particle with only one decay mode providing dark matter with the desired free-streaming scale. They found much smaller  $\delta$ s than required by the consistent production of dark radiation, cf. Sec. 2. Their numerical results agree with those obtained from our formulae (38) and (41).

We use the general result (37) for the free-streaming scale of a particle emitted with relativistic momentum. Inserting as below (37) with the only difference in  $T_2^{\text{nr}}$ , which is given, here, by (50), the free-streaming scale  $\lambda_2^{\text{fs}}$  of the heavier daughters as function of  $x_2$  and the time of decay is just (38) with the replacement  $\frac{(\delta+1)^2-1}{\delta+1} \rightarrow (x_2^{-2}-4)^{\frac{1}{2}}$ . This can be read as implicit equation for  $x_2$  arising from constraints on its free-streaming scale or to obtain a desired free-streaming scale to solve the missing satellites problem, for example. It is

$$\begin{aligned} \frac{\lambda_2^{\text{fs}}(x_2, \tau)}{0.4 \text{ Mpc}} &\approx 0.23 \left( \frac{\tau}{10^7 \text{ s}} \right)^{\frac{1}{2}} (x_2^{-2} - 4)^{\frac{1}{2}} \frac{(g_*^{\text{d}})^{1/4}}{(g_*^{\text{nr}})^{1/2}} \left( \frac{(g_{*s}^{\text{nr}})^2}{g_{*s}^{\text{d}} g_{*s}^0} \right)^{\frac{1}{3}} \\ &\times \left\{ 5 - \frac{4}{\mu} (x_2^{-2} - 4)^{-\frac{1}{2}} \left( \frac{g_*^{\text{nr}}}{g_*^{\text{d}}} \right)^{\frac{1}{4}} \left( \frac{g_{*s}^{\text{d}}}{g_{*s}^{\text{nr}}} \right)^{\frac{1}{3}} \right. \\ &\left. + \ln \left[ \frac{t_{\text{eq}}}{\tau} \frac{4}{\mu^2} (x_2^{-2} - 4)^{-1} \left( \frac{g_*^{\text{nr}}}{g_*^{\text{d}}} \right)^{\frac{1}{2}} \left( \frac{g_{*s}^{\text{d}}}{g_{*s}^{\text{nr}}} \right)^{\frac{2}{3}} \right] \right\}. \end{aligned} \quad (58)$$

To obtain the thick solid curve in Fig. 12 we solved (58) numerically. Equally well, one can read off the required time of decay from Fig. 12, if  $x_2$  is set by the particle physics

model. Overplotted as very thin grey curve is the simple analytic approximation

$$x_2 \simeq \frac{2}{\sqrt{\pi}} \left( \frac{0.4 \text{ Mpc}}{\lambda_2^{\text{fs}}} \right)^{1.21} \left( \frac{\tau}{10^7 \text{ s}} \right)^{0.5}. \quad (59)$$

For  $\lambda_2^{\text{fs}} = 0.4 \text{ Mpc}$  it is barely visible except very close to  $8 \times 10^5 \text{ s}$ . For  $\lambda_2^{\text{fs}} = 10 \text{ Mpc}$  it is slightly too small, while for  $\lambda_2^{\text{fs}} = 100 \text{ Mpc}$  the fit is again almost perfect.

In order to find an analytic estimate we first simplify (58) by omitting relativistic free-streaming and free-streaming after  $t_{\text{eq}}$ . Exploiting logarithm rules we can see that one might neglect the factor  $(x_2^{-2} - 4)^{-1}$  in the logarithm, if  $x_2 \gg (\mu/2)(\tau/t_{\text{eq}})^{1/2}(g_*^{\text{d}}/g_*^{\text{nr}})^{1/4}(g_{*s}^{\text{nr}}/g_{*s}^{\text{d}})^{1/3}$ , which holds for decays sufficiently earlier than  $t_{\text{eq}}$ . Then  $x_2$  can be singled out to obtain

$$x_2 \simeq \left[ \left( 0.23 \frac{0.4 \text{ Mpc}}{\lambda_2^{\text{fs}}} \left( \frac{\tau}{10^7 \text{ s}} \right)^{\frac{1}{2}} \frac{(g_*^{\text{d}})^{\frac{1}{4}}}{(g_{*s}^{\text{nr}})^{\frac{1}{2}}} \left( \frac{(g_{*s}^{\text{nr}})^2}{g_{*s}^0 g_{*s}^{\text{d}}} \right)^{\frac{1}{3}} \right. \right. \\ \left. \left. \times \ln \left[ \frac{t_{\text{eq}}}{\tau} \frac{4}{\mu} \left( \frac{g_*^{\text{nr}}}{g_*^{\text{d}}} \right)^{\frac{1}{2}} \left( \frac{g_{*s}^{\text{d}}}{g_{*s}^{\text{nr}}} \right)^{\frac{2}{3}} \right] \right)^{-2} + 4 \right]^{-\frac{1}{2}}, \quad (60)$$

where  $g_*^{\text{nr}} = g_*^0$  and  $g_{*s}^{\text{nr}} = g_{*s}^0$  for  $\lambda_2^{\text{fs}} = 0.4 \text{ Mpc}$ . As can be seen in Fig. 12 the result is systematically too large and the logarithmic dependence is misleading. On the other hand we find the dependence on  $\tau$  and a very weak dependence on  $g_*^{\text{d}}$ . The shift with  $\lambda_2^{\text{fs}}$  is well reproduced.

The corresponding time when the heavier daughters become non-relativistic is  $\sim 3.4 \times 10^6 \text{ s}$ . So this event appears rather unobservable. It is not a surprise that we find a constant value, because in this case  $\lambda_{\text{fs}} = 0.4 \text{ Mpc}$  is set by  $t_2^{\text{nr}}$  as argued below (37). With the analytic result (60) we can verify the dependence of  $t_2^{\text{nr}}$  on  $g_*^{\text{d}}$ . It is weaker than  $\propto (g_*^{\text{d}})^{1/6}$  and mainly due to the change in the contribution from relativistic free-streaming.

Inserting the desired  $x_2$  into the non-dominance requirement (56) at the boundary, so that the heavier daughters actually have to form the observed dark matter, yields the unique branching ratio  $B_2$  to produce the desired dark radiation and the dark matter of the Universe with the desired free-streaming scale at the same time from the same late decaying particle. We find a constant value,

$$B_2 \simeq 5.5 \times 10^{-3} \left( \frac{\lambda_2^{\text{fs}}}{0.4 \text{ Mpc}} \right) \Delta N_{\text{eff}}^{-1} \left( \frac{\Omega_{\text{dm}} h^2}{0.1246} \right), \quad (61)$$

with an even weaker dependence on  $g_*$  as  $t_2^{\text{nr}}$ . This is no longer a surprise, because with fix  $t_2^{\text{nr}}$  also  $B_2$  becomes fixed in order for the heavier daughters to form the observed dark matter. Taking into account uncertainties  $7.8 \times 10^{-4} \lesssim B_2 \lesssim 2.7 \times 10^{-2}$ . In the course we had to discard the second solution to (58) as unphysical. To obtain an analytic estimate we insert (60) into (56) and single out

$$B_2 \simeq \frac{1}{B_2^{-1} - 1} = 0.039 \left( \frac{\lambda_2^{\text{fs}}}{0.4 \text{ Mpc}} \right) \Delta N_{\text{eff}}^{-1} \left( \frac{\Omega_{\text{dm}} h^2}{0.1246} \right) \ln \left[ \frac{t_{\text{eq}}}{\tau} \frac{4}{\mu^2} \left( \frac{g_*^{\text{nr}}}{g_*^{\text{d}}} \right)^{\frac{1}{2}} \left( \frac{g_{*s}^{\text{d}}}{g_{*s}^{\text{nr}}} \right)^{\frac{2}{3}} \right]^{-1}, \quad (62)$$

where we took  $1 - 4x_1^2 \simeq 1$  assuming sufficiently small  $x_1$  and, again,  $g_*^{\text{nr}} = g_*^0$  and  $g_{*s}^{\text{nr}} = g_{*s}^0$ . The logarithmic dependence is misleading, while the dependencies on  $\lambda_2^{\text{fs}}$ ,  $\Delta N_{\text{eff}}$  and  $\Omega_{\text{dm}} h^2$  in (61) find a reason.

#### 4.4 Hot dark matter opportunity

In this section we point out the same hot dark matter opportunity as at the end of Sec. 2.3.2 but for the case of two dark decay modes. To be able to lead to a non-zero cosmological neutrino mass scale like  $\sum m_\nu = 0.34$  eV inferred from the cluster abundance as in [48] the free-streaming scale of the heavier daughters must be larger than the corresponding structure formation scale,  $\lambda_2^{\text{fs}} > \lambda_{\text{gc}} \sim 10$  Mpc. As before we solved (58) numerically to obtain the required mass hierarchy  $x_2$  as depicted in Fig. 12 to have  $\lambda_2^{\text{fs}} \simeq 10$  Mpc. The corresponding times for the heavier daughters to become non-relativistic are  $t_2^{\text{nr}}(\lambda_2^{\text{fs}} = 10 \text{ Mpc}) \simeq 2.4 \times 10^9$  s and  $t_2^{\text{nr}}(\lambda_2^{\text{fs}} = 100 \text{ Mpc}) \simeq 8.6 \times 10^{11}$  s. Thus only for very large free-streaming scales they become non-relativistic after  $\tau_{\text{cmb}}^{\text{max}}$ . Inserting the found  $x_2$  into (56) with the replacement  $\Omega_{\text{dm}} \rightarrow \Omega_{\text{hdm}} = b_{\text{max}}(\sum m_\nu)\Omega_{\text{dm}} \sim 0.033 \Omega_{\text{dm}}$  we find at the boundary the corresponding branching ratio into the heavier daughters  $B_2$  to obtain  $\Delta N_{\text{eff}} = 0.86$  and  $\sum m_\nu = 0.34$  eV from the same particle decay. In order to act as the dark radiation we assume the lighter daughters to be still relativistic today with the corresponding mass hierarchy  $x_1$  given by (51). We find a constant branching ratio

$$B_2 \simeq 10^{-2} \left( \frac{\lambda_2^{\text{fs}}}{10 \text{ Mpc}} \right) \left( \frac{b_{\text{max}}}{0.033} \right) \Delta N_{\text{eff}}^{-1} \left( \frac{\Omega_{\text{dm}} h^2}{0.1246} \right). \quad (63)$$

Larger free-streaming scales are possible or might be preferred. At  $\lambda_2^{\text{fs}} = 100$  Mpc the approximation (63) is significantly smaller than the true value  $\sim 0.175$ . In any case, it is trivial to solve (56) with the appropriate replacements for any fixed value of  $x_2$ . The allowed area of values  $x_2(\tau)$  is found above the thick dash-dotted curve in Fig. 12.

Altogether, we have shown that any desired amount of hot dark matter and dark radiation can originate from the same decay, while in the case of two dark decay modes the relative branching ratio allows to vary the time the hot dark matter becomes non-relativistic. This time determines the HDM free-streaming scale. It is relatively small, if they become non-relativistic before  $\tau_{\text{cmb}}^{\text{max}}$  and larger, if they become non-relativistic after  $\tau_{\text{cmb}}^{\text{max}}$ . In the case of massive neutrinos and also in the case of HDM from particle decay with only one dark decay mode, this time is much later than  $t_{\text{eq}}$ . This offers a possibility to differ between these cases in cosmological observations.

## 5 Results and conclusions

We studied particle decay as the origin of dark radiation. After elaborating general properties of such cosmologies we determined model-independent constraints on possible underlying theories. Since the energy density of the decaying particle is fixed by the amount of dark radiation and thus by observations independent of an underlying particle physics model, bounds on branching ratios and constraints on the mass hierarchies

between decaying particle and decay products depend in a unique way on the time of decay.

If the decaying particle possesses only one dark decay mode, we find that the minimal free-streaming scale of its decay products is so large that hot dark matter constraints apply to their relic densities. Therefore, the heavier decay product in a particle decay producing the desired dark radiation cannot form the observed dark matter. So hot dark matter constraints determine the minimal mass hierarchy between decaying particle and the heavier decay product. This constraint is depicted in Fig. 2, where also cosmology-specific uncertainties are shown. The hot dark matter bound is the tightest bound obtainable taking into account the impact of the scenario on structure formation. On the other hand, a hot dark matter component in excess of the SM neutrinos could not only have originated from particle decay but also share its origin with the desired dark radiation. The heavier decay product can form a finite hot dark matter component, while the lighter one acts as dark radiation. In any case decay products become non-relativistic during or after CMB times.

If the decaying particle possesses two dark decay modes, the free-streaming scales of the decay products are set and can be adjusted by the involved couplings and masses. Therefore, there are not only constraints, as shown in Fig. 11, but also additional opportunities arising from the impact of the heavier decay products on structure formation. Depending on the time of decay we provide the unique mass hierarchy and relative branching to produce dark radiation and dark matter with any desired free-streaming scale from the same particle decay. The observed dark matter satisfying the cold dark matter paradigm may have originated from such a decay. Any finite hot dark matter contribution can be explained and possibly be distinguished in future cosmological observations from other sources like SM neutrinos. In a different range of mass hierarchies and the corresponding branching ratios, the dark matter from particle decay solves the missing satellites problem.

We determined general upper bounds on several branching ratios of the decaying particle into decay products with SM interactions. These are independent of the underlying theory and, for example, independent of the number of dark decay modes. Direct decays are constrained as shown in Figs. 4, 5 and 6. Since these constraints are severe, we considered scenarios fulfilling them by construction. Dangerous terms in the Lagrangian are forbidden by kinematics or by symmetries. However, after taking into account the amount of energy that is always carried away invisibly we find that also off-shell and loop processes are severely constrained, cf. Figs. 7, 8 and 9. A certain finite branching ratio into hadronically interacting particles could solve the cosmic lithium problems. The emission of photons may enable future CMB polarimeters to detect and identify the desired cosmological particle decay. More robustly, the obtained bounds have the power to exclude many particle physics scenarios. As an example we show how decays of the lightest ordinary supersymmetric particle into an invisible particle like the gravitino are excluded as the origin of the desired dark radiation during and after BBN. We argue that particle decay as origin of dark radiation serves as a motivation to extend existing studies of constraints on cosmological particle decays towards smaller masses of the decaying particle. For example, BBN constraints do not seem to apply to a particle

that freezes out relativistically and produces the desired dark radiation in its necessarily late decay during or after BBN.

Since we provide simple analytic formulae and figures pointing out uncertainties, our results can easily be adopted to constrain particle physics models and as a guideline for model building. Particle decay as the origin of dark radiation raises very specific requirements on any underlying theory. Most existing proposals assume implicitly that constraints are satisfied. Often decaying particle and decay products have only extremely weak interactions. Thus, they safely satisfy branching ratio constraints but cannot lead to additional observable consequences.

We point out various opportunities of a cosmological particle decay serving as a motivation for further studies. There is a plethora of possible cosmologies to be explored. As close as some interplay between the different mysteries of our universe is, as attractive appears a theory that combines and intertwines them.

## Acknowledgements

We thank Steen Hannestad, Jan Hamann, Raul Jimenez and Licia Verde for valuable discussions. We especially thank Torsten Bringmann for sharing his expertise. This work was supported by the German Research Foundation (DFG) via the Junior Research Group ‘‘SUSY Phenomenology’’ within the Collaborative Research Centre 676 ‘‘Particles, Strings and the Early Universe’’.

## A Exponential decay in an expanding universe

Any initial momentum  $p_{\text{ini}}$  from a decay is red-shifted by the expansion of the Universe. It is

$$p(t, t_0) = p_{\text{ini}} \frac{a(t)}{a(t_0)} = p_{\text{ini}} \left( \frac{t}{t_0} \right)^{\frac{2}{3(1+\omega)}}. \quad (64)$$

How the scale factor  $a \propto t^{\frac{2}{3(1+\omega)}}$  grows with time depends on the equation of state of the Universe,  $p = \omega\rho$  with  $\omega = 1/3$  if it is radiation dominated and  $\omega = 0$  in the case of matter domination. Earlier emitted particles experience a longer time of expansion and thus more red-shift than later emitted particles. Taking into account the exponential decay law this leads to a more involved momentum distribution than the monochromatic line obtained in the sudden decay approximation.

Two-body decays have no intrinsic momentum distribution. In this case the momentum distribution function  $f(p, t_0)$  of an emitted particle is determined by the number of produced particles in a given time interval  $dt$  at time  $t$ . It is

$$N \frac{dt}{\tau} = f(p, t_0) dp, \quad (65)$$

if  $N(t) = N_0 e^{-t/\tau}$  is the number of decaying particles. If the number of dark radiation particles produced in each decay  $g_{\text{dr}} \neq 1$ , we replace  $N \rightarrow g_{\text{dr}} N$ . So

$$f(p, t_0) = \frac{N}{\tau} \frac{dt}{dp} \quad (66)$$

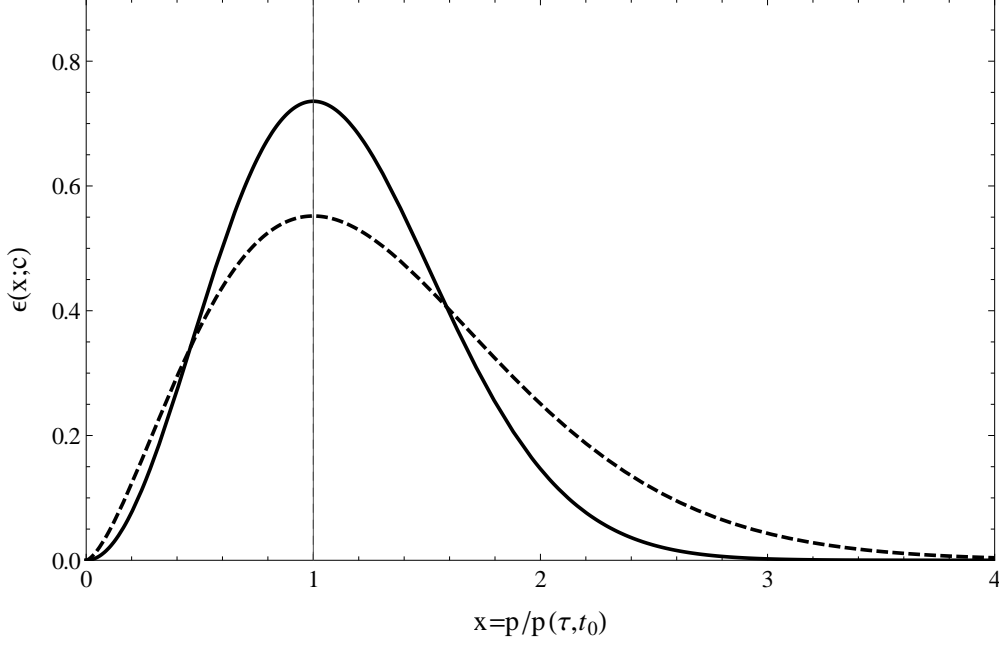


Figure 13: Normalised, time-invariant energy spectrum  $\epsilon(x = p/p(\tau, t_0); c)$  of relativistic particles from two-body decay (decaying particle at rest) in an expanding Universe with scale factor  $a \propto t^{1/c}$ . The solid (dashed) line is obtained from (74) as described in the text with  $c = 2(3/2)$ . The maximum of the energy spectra is highlighted at  $x = 1 \Leftrightarrow p = p(\tau, t_0)$ .

and reversing (64) we can insert  $t(p, t_0)$ , which gives  $dt/dp$  as well, also in  $N(t)$  arriving at

$$\begin{aligned} f(p, t_0) &= cN_0 p^{-c}(\tau, t_0) e^{-\left(\frac{p}{p(\tau, t_0)}\right)^c} p^{c-1} \\ &= cN_0 p^{-1} \frac{t_0}{\tau} \left(\frac{p}{p_{\text{ini}}}\right)^c e^{-\frac{t_0}{\tau} \left(\frac{p}{p_{\text{ini}}}\right)^c}, \end{aligned} \quad (67)$$

where we abbreviated  $c \equiv 3(1 + \omega)/2 > 0$ . With the assumption of a constant  $\omega$  we do not include the case of a particle that shortly dominates the energy density of the Universe at its decay during radiation domination. As argued in the text this situation is not expected to occur.

**Total energy** Since dark radiation particles are relativistic, each particle's energy is given by its kinetic energy, so its momentum,  $E \simeq p$ . The total energy in dark radiation is thus given by the integral

$$E_{\text{dr}}(t_0) = \int_0^{p_{\text{ini}}} p f(p, t_0) dp. \quad (68)$$

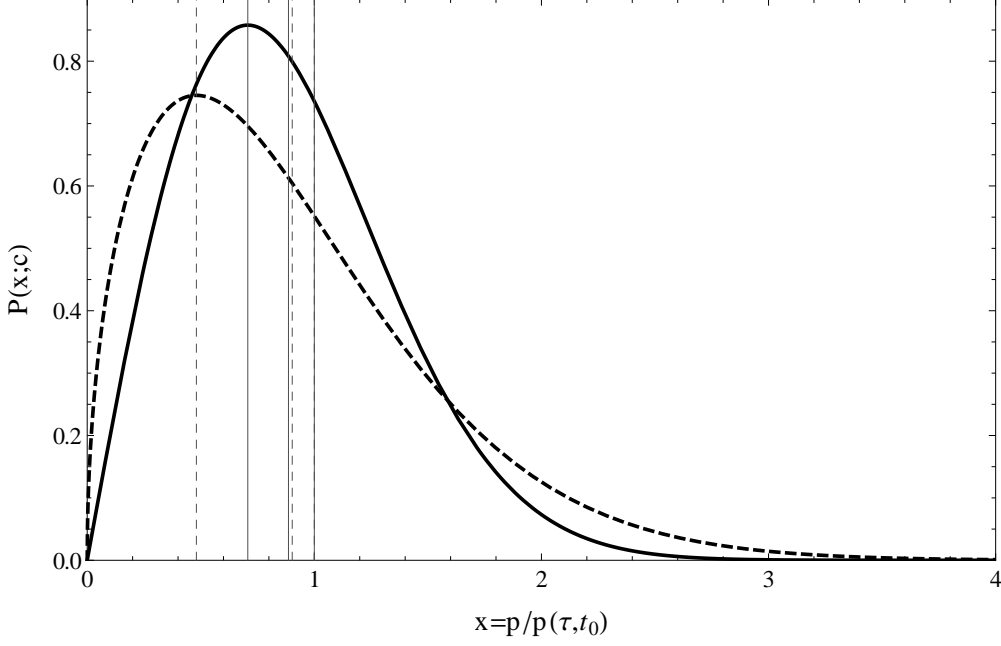


Figure 14: Normalised, time-invariant probability distribution  $P(x; c) = cx^{c-1}e^{-x^c}$  of (76) for finding a relativistic particle from two-body decay (decaying particle at rest) within the infinitesimal momentum interval  $[p, p+\delta p]$ . The solid (dashed) line is obtained for  $c = 2(3/2)$ . Vertical lines highlight the maxima of the corresponding distributions,  $x \simeq 0.707$  ( $c = 2$ ) and  $x \simeq 0.481$  ( $c = 3/2$ ), as well as the mean of the distributions,  $\mu = \sqrt{\pi}/2$  ( $c = 2$ ) and  $\mu = \Gamma[2/3]2/3$  ( $c = 3/2$ ). The maximum of the corresponding energy spectra is at  $x = 1$ , cf. Fig. 13.

Inserting (67) for  $c > 0$  this becomes

$$E_{\text{dr}}(t_0) = N_0 p(\tau, t_0) \frac{1}{c} \left( \Gamma\left[\frac{1}{c}\right] - c \Gamma\left[1 + \frac{1}{c}, \frac{t_0}{\tau}\right] \right), \quad (69)$$

where  $\Gamma[z]$  denotes the Euler gamma function and  $\Gamma[a, z]$  the incomplete gamma function. In the case of radiation domination ( $c = 2$ ) (69) reduces to

$$E_{\text{dr}}(t_0) = N_0 p(\tau, t_0) \left( \frac{\sqrt{\pi}}{2} \text{Erf}\left[\left(\frac{t_0}{\tau}\right)^{\frac{1}{2}}\right] - \left(\frac{t_0}{\tau}\right)^{\frac{1}{2}} e^{-\frac{t_0}{\tau}} \right), \quad (70)$$

where  $\text{Erf}[z]$  denotes the error function.

Times of interest are later than the time of decay, so that we should investigate the limit  $t_0 \gg \tau$ . In this limit the general expression (69) yields

$$\lim_{t_0 \gg \tau} E_{\text{dr}}(t_0) = N_0 p(\tau, t_0) \frac{1}{c} \Gamma\left[\frac{1}{c}\right]. \quad (71)$$



The difference by taking into account the exponential decay behaviour in contrast to the sudden decay approximation is thus found in the factor  $c^{-1}\Gamma[c^{-1}]$ . For the two important cases this is

$$\mu = \frac{\sqrt{\pi}}{2} \simeq 0.886 \quad \text{in radiation domination, } c = 2, \quad (72)$$

and

$$\mu = \frac{2}{3}\Gamma[\frac{2}{3}] \simeq 0.902 \quad \text{in matter domination, } c = 3/2. \quad (73)$$

The difference in (71) between these cases is thus below two percent. However, compared to the sudden decay approximation it is twelve percent.

**Invariant energy spectrum** The integral of the momentum distribution function  $f(p, t_0)$  over full parameter space yields the total number of particles  $g_{\text{dr}}N_0$ . The integral of the energy spectrum  $\epsilon$  over full parameter space yields the total energy (68) and is thus just found as

$$\epsilon(p, t_0) = pf(p, t_0). \quad (74)$$

The effect of red-shift is easily comprehensible. At times  $t_0 \gg \tau$  it is an equal shift of all momenta towards smaller ones, which does not change the characteristic form developed roughly until  $t_0 \sim 3\tau$  and  $t_0 \sim 4\tau$ , respectively. Therefore, we give the normalised and time-invariant energy spectrum  $\epsilon(x)$  in Fig. 13 by defining  $x = p/p(\tau, t_0)$ .

We treat the non-relativistic decaying particle to be at rest. The correction from a non-zero kinetic energy is negligible, if the decaying particle has a sufficiently small momentum. This is the case for all considered scenarios in this work.

**Probability distribution** Determining the probability distribution  $P(p, t_0)$  for finding a particle within an infinitesimal momentum interval  $[p, p + \delta p]$  we note that by construction

$$1 \stackrel{!}{=} \int_0^\infty P(p, t_0) dp = \int_0^\infty \frac{f(p, t_0)}{N_0} dp. \quad (75)$$

Thus we have also just found  $P(p, t_0)$ . Performing the same change of coordinates as for the energy spectrum,  $p \rightarrow x = p/p(\tau, t_0)$ , we obtain

$$\int_0^\infty P(x) dx = \int_0^\infty cx^{c-1} e^{-x^c} dx. \quad (76)$$

This time-invariant distribution is depicted in Fig. 14. Highlighted are the maximum of the corresponding energy spectrum at  $x = 1$ , which is independent of  $c$ , the maximum of the distribution itself at  $x \simeq 0.707$  ( $c = 2$ ),  $x \simeq 0.481$  ( $c = 3/2$ ) and the mean of the distribution

$$\mu(P) = \int_0^\infty xP(x) dx = c^{-1}\Gamma[c^{-1}] \quad (77)$$

to compare with (71). Obviously,  $P(x)$  is asymmetric. The variance  $\phi(P)$  also known as the second moment of  $P$  is found as

$$\phi(P) = \int_0^\infty (x - \mu)^2 P(x) dx = \Gamma[1 + \frac{2}{c}] - \mu^2 \simeq \begin{cases} 0.215 & \text{for } c = 2 \\ 0.376 & \text{for } c = 3/2 \end{cases}. \quad (78)$$

The difference in  $\phi$  is thus about 55% and compared to the sudden decay approximation like a factor of 5 in the case of radiation domination.

## References

- [1] Y. I. Izotov and T. X. Thuan, “The primordial abundance of  $^4\text{He}$ : evidence for non-standard big bang nucleosynthesis”, *Astrophys. J.* **710** (2010) L67–L71, [arXiv:1001.4440](#) [[astro-ph.CO](#)].
- [2] E. Aver, K. A. Olive, and E. D. Skillman, “A New Approach to Systematic Uncertainties and Self-Consistency in Helium Abundance Determinations”, *JCAP* **1005** (2010) 003, [arXiv:1001.5218](#).
- [3] G. Mangano and P. D. Serpico, “A robust upper limit on  $N_{\text{eff}}$  from BBN, circa 2011”, *Phys.Lett.* **B701** (2011) 296–299, [arXiv:1103.1261](#) [[astro-ph.CO](#)].
- [4] R. Bowen, S. H. Hansen, A. Melchiorri, J. Silk, and R. Trotta, “The Impact of an Extra Background of Relativistic Particles on the Cosmological Parameters derived from Microwave Background Anisotropies”, *Mon. Not. Roy. Astron. Soc.* **334** (2002) 760, [arXiv:astro-ph/0110636](#).
- [5] R. Keisler *et al.*, “A Measurement of the Damping Tail of the Cosmic Microwave Background Power Spectrum with the South Pole Telescope”, *Astrophys.J.* **743** (2011) 28, [arXiv:1105.3182](#) [[astro-ph.CO](#)].
- [6] J. Dunkley, R. Hlozek, J. Sievers, V. Acquaviva, P. Ade, *et al.*, “The Atacama Cosmology Telescope: Cosmological Parameters from the 2008 Power Spectra”, *Astrophys.J.* **739** (2011) 52, [arXiv:1009.0866](#) [[astro-ph.CO](#)].
- [7] Z. Hou, R. Keisler, L. Knox, M. Millea, and C. Reichardt, “How Massless Neutrinos Affect the Cosmic Microwave Background Damping Tail”, [arXiv:1104.2333](#) [[astro-ph.CO](#)].
- [8] E. Kawakami, M. Kawasaki, K. Miyamoto, K. Nakayama, and T. Sekiguchi, “Non-Gaussian isocurvature perturbations in dark radiation”, *JCAP* **1207** (2012) 037, [arXiv:1202.4890](#) [[astro-ph.CO](#)].
- [9] K. T. Mehta, A. J. Cuesta, X. Xu, D. J. Eisenstein, and N. Padmanabhan, “A 2% Distance to  $z = 0.35$  by Reconstructing Baryon Acoustic Oscillations - III : Cosmological Measurements and Interpretation”, [arXiv:1202.0092](#) [[astro-ph.CO](#)].
- [10] E. Calabrese, M. Archidiacono, A. Melchiorri, and B. Ratra, “The impact of a new median statistics  $H_0$  prior on the evidence for dark radiation”, *Phys.Rev.* **D86** (2012) 043520, [arXiv:1205.6753](#) [[astro-ph.CO](#)].

- [11] S. Bashinsky and U. Seljak, “Signatures of relativistic neutrinos in CMB anisotropy and matter clustering”, *Phys. Rev.* **D69** (2004) 083002, [arXiv:astro-ph/0310198](#).
- [12] J. Hamann, S. Hannestad, G. G. Raffelt, and Y. Y. Y. Wong, “Observational bounds on the cosmic radiation density”, *JCAP* **0708** (2007) 021, [arXiv:0705.0440 \[astro-ph\]](#).
- [13] M. Gonzalez-Garcia, M. Maltoni, and J. Salvado, “Robust Cosmological Bounds on Neutrinos and their Combination with Oscillation Results”, *JHEP* **1008** (2010) 117, [arXiv:1006.3795 \[hep-ph\]](#).
- [14] E. Calabrese, D. Huterer, E. V. Linder, A. Melchiorri, and L. Pagano, “Limits on Dark Radiation, Early Dark Energy, and Relativistic Degrees of Freedom”, *Phys. Rev.* **D83** (2011) 123504, [arXiv:1103.4132 \[astro-ph.CO\]](#).
- [15] A. X. Gonzalez-Morales, R. Poltis, B. D. Sherwin, and L. Verde, “Are priors responsible for cosmology favoring additional neutrino species?”, [arXiv:1106.5052 \[astro-ph.CO\]](#).
- [16] M. Moresco, L. Verde, L. Pozzetti, R. Jimenez, and A. Cimatti, “New constraints on cosmological parameters and neutrino properties using the expansion rate of the Universe to  $z \sim 1.75$ ”, [arXiv:1201.6658 \[astro-ph.CO\]](#).
- [17] S. Joudaki, “Constraints on Neutrino Mass and Light Degrees of Freedom in Extended Cosmological Parameter Spaces”, [arXiv:1202.0005 \[astro-ph.CO\]](#).
- [18] M. Archidiacono, E. Giusarma, A. Melchiorri, and O. Mena, “Dark Radiation in extended cosmological scenarios”, *Phys.Rev.* **D86** (2012) 043509, [arXiv:1206.0109 \[astro-ph.CO\]](#).
- [19] L. Perotto, J. Lesgourgues, S. Hannestad, H. Tu, and Y. Y. Y. Wong, “Probing cosmological parameters with the CMB: Forecasts from full Monte Carlo simulations”, *JCAP* **0610** (2006) 013, [arXiv:astro-ph/0606227](#).
- [20] J. Hamann, J. Lesgourgues, and G. Mangano, “Using BBN in cosmological parameter extraction from CMB: a forecast for Planck”, *JCAP* **0803** (2008) 004, [arXiv:0712.2826 \[astro-ph\]](#).
- [21] J. Hamann, S. Hannestad, G. G. Raffelt, I. Tamborra, and Y. Y. Y. Wong, “Cosmology seeking friendship with sterile neutrinos”, *Phys.Rev.Lett.* **105** (2010) 181301, [arXiv:1006.5276 \[hep-ph\]](#).
- [22] K. Abazajian *et al.*, “Light Sterile Neutrinos: A White Paper”, [arXiv:1204.5379 \[hep-ph\]](#).
- [23] A. Mirizzi, N. Saviano, G. Miele, and P. D. Serpico, “Light sterile neutrino production in the early universe with dynamical neutrino asymmetries”, *Phys.Rev.* **D86** (2012) 053009, [arXiv:1206.1046 \[hep-ph\]](#).

- [24] L. A. Anchordoqui, H. Goldberg, and G. Steigman, “Right-Handed Neutrinos as the Dark Radiation: Status and Forecasts for the LHC”, [arXiv:1211.0186 \[hep-ph\]](#).
- [25] J. Jaeckel, J. Redondo, and A. Ringwald, “Signatures of a hidden cosmic microwave background”, *Phys.Rev.Lett.* **101** (2008) 131801, [arXiv:0804.4157 \[astro-ph\]](#).
- [26] K. Nakayama, F. Takahashi, and T. T. Yanagida, “A theory of extra radiation in the Universe”, *Phys.Lett.* **B697** (2011) 275–279, [arXiv:1010.5693 \[hep-ph\]](#).
- [27] J. L. Feng, V. Renteria, and Z. Surujon, “WIMPless Dark Matter in Anomaly-Mediated Supersymmetry Breaking with Hidden QED”, *Phys.Rev.* **D84** (2011) 095033, [arXiv:1108.4689 \[hep-ph\]](#).
- [28] S. Chang and H. B. Kim, “A dark matter solution from the supersymmetric axion model”, *Phys. Rev. Lett.* **77** (1996) 591–594, [arXiv:hep-ph/9604222](#).
- [29] J. Hasenkamp and J. Kersten, “Dark and visible matter with broken R-parity and the axion multiplet”, *Phys.Lett.* **B701** (2011) 660–666, [arXiv:1103.6193 \[hep-ph\]](#).
- [30] K. S. Jeong and F. Takahashi, “Light Higgsino from Axion Dark Radiation”, *JHEP* **1208** (2012) 017, [arXiv:1201.4816 \[hep-ph\]](#).
- [31] P. Graf and F. D. Steffen, “Axions and saxions from the primordial supersymmetric plasma and extra radiation signatures”, [arXiv:1208.2951 \[hep-ph\]](#).
- [32] M. Cicoli, J. P. Conlon, and F. Quevedo, “Dark Radiation in LARGE Volume Models”, [arXiv:1208.3562 \[hep-ph\]](#).
- [33] T. Higaki and F. Takahashi, “Dark Radiation and Dark Matter in Large Volume Compactifications”, *JHEP* **1211** (2012) 125, [arXiv:1208.3563 \[hep-ph\]](#).
- [34] K. Ichikawa, M. Kawasaki, K. Nakayama, M. Senami, and F. Takahashi, “Increasing effective number of neutrinos by decaying particles”, *JCAP* **0705** (2007) 008, [arXiv:hep-ph/0703034](#).
- [35] W. Fischler and J. Meyers, “Dark Radiation Emerging After Big Bang Nucleosynthesis?”, *Phys.Rev.* **D83** (2011) 063520, [arXiv:1011.3501 \[astro-ph.CO\]](#).
- [36] J. Hasenkamp, “Dark radiation from the axino solution of the gravitino problem”, *Phys. Lett.* **B707** (2012) 121–128, [arXiv:1107.4319 \[hep-ph\]](#).
- [37] G. M. Fuller, C. T. Kishimoto, and A. Kusenko, “Heavy sterile neutrinos, entropy and relativistic energy production, and the relic neutrino background”, [arXiv:1110.6479 \[astro-ph.CO\]](#).

- [38] J. L. Menestrina and R. J. Scherrer, “Dark Radiation from Particle Decays during Big Bang Nucleosynthesis”, *Phys.Rev.* **D85** (2012) 047301, [arXiv:1111.0605 \[astro-ph.CO\]](#).
- [39] D. Hooper, F. S. Queiroz, and N. Y. Gnedin, “Nonthermal dark matter mimicking an additional neutrino species in the early universe”, *Phys.Rev.* **D85** (2012) 063513, [arXiv:1111.6599 \[astro-ph.CO\]](#).
- [40] O. E. Bjælde, S. Das, and A. Moss, “Origin of  $\Delta N_{\text{eff}}$  as a Result of an Interaction between Dark Radiation and Dark Matter”, *JCAP* **1210** (2012) 017, [arXiv:1205.0553 \[astro-ph.CO\]](#).
- [41] K. Choi, K.-Y. Choi, and C. S. Shin, “Dark radiation and small-scale structure problems with decaying particles”, *Phys.Rev.* **D86** (2012) 083529, [arXiv:1208.2496 \[hep-ph\]](#).
- [42] M. Gonzalez-Garcia, V. Niro, and J. Salvado, “Dark Radiation and Decaying Matter”, [arXiv:1212.1472 \[hep-ph\]](#).
- [43] C. Boehm, M. J. Dolan, and C. McCabe, “Increasing  $N_{\text{eff}}$  with particles in thermal equilibrium with neutrinos”, [arXiv:1207.0497 \[astro-ph.CO\]](#).
- [44] R. Jinno, T. Moroi, and K. Nakayama, “Probing dark radiation with inflationary gravitational waves”, [arXiv:1208.0184 \[astro-ph.CO\]](#).
- [45] K. Jedamzik, “Lithium-6: A Probe of the Early Universe”, *Phys.Rev.Lett.* **84** (2000) 3248, [arXiv:astro-ph/9909445](#).
- [46] A. A. Klypin, A. V. Kravtsov, O. Valenzuela, and F. Prada, “Where are the missing Galactic satellites?”, *Astrophys.J.* **522** (1999) 82–92, [arXiv:astro-ph/9901240](#).
- [47] B. Moore, S. Ghigna, F. Governato, G. Lake, T. R. Quinn, *et al.*, “Dark matter substructure within galactic halos”, *Astrophys.J.* **524** (1999) L19–L22, [arXiv:astro-ph/9907411](#).
- [48] B. Benson *et al.*, “Cosmological Constraints from Sunyaev-Zel’dovich-Selected Clusters with X-ray Observations in the First 178 Square Degrees of the South Pole Telescope Survey”, [arXiv:1112.5435 \[astro-ph.CO\]](#).
- [49] G. Mangano *et al.*, “Relic neutrino decoupling including flavour oscillations”, *Nucl. Phys.* **B729** (2005) 221–234, [arXiv:hep-ph/0506164](#).
- [50] WMAP Collaboration, E. Komatsu *et al.*, “Seven-Year Wilkinson Microwave Anisotropy Probe (WMAP) Observations: Cosmological Interpretation”, *Astrophys.J.Suppl.* **192** (2011) 18, [arXiv:1001.4538 \[astro-ph.CO\]](#).
- [51] Particle Data Group, J. Beringer *et al.*, “Review of Particle Physics (RPP)”, *Phys.Rev.* **D86** (2012) 010001.

- [52] D. J. Eisenstein and W. Hu, “Baryonic features in the matter transfer function”, *Astrophys.J.* **496** (1998) 605, [arXiv:astro-ph/9709112](#).
- [53] J. Hamann, S. Hannestad, G. G. Raffelt, and Y. Y. Wong, “Sterile neutrinos with eV masses in cosmology: How disfavoured exactly?”, *JCAP* **1109** (2011) 034, [arXiv:1108.4136 \[astro-ph.CO\]](#).
- [54] S. Joudaki, K. N. Abazajian, and M. Kaplinghat, “Are Light Sterile Neutrinos Preferred or Disfavored by Cosmology?”, [arXiv:1208.4354 \[astro-ph.CO\]](#).
- [55] U. Seljak, A. Makarov, P. McDonald, and H. Trac, “Can sterile neutrinos be the dark matter?”, *Phys.Rev.Lett.* **97** (2006) 191303, [arXiv:astro-ph/0602430](#).
- [56] M. Viel, J. Lesgourgues, M. G. Haehnelt, S. Matarrese, and A. Riotto, “Can sterile neutrinos be ruled out as warm dark matter candidates?”, *Phys.Rev.Lett.* **97** (2006) 071301, [arXiv:astro-ph/0605706](#).
- [57] M. Viel, G. D. Becker, J. S. Bolton, M. G. Haehnelt, M. Rauch, *et al.*, “How cold is cold dark matter? Small scales constraints from the flux power spectrum of the high-redshift Lyman-alpha forest”, *Phys.Rev.Lett.* **100** (2008) 041304, [arXiv:0709.0131 \[astro-ph\]](#).
- [58] K. Abazajian, “Linear cosmological structure limits on warm dark matter”, *Phys.Rev.* **D73** (2006) 063513, [arXiv:astro-ph/0512631](#).
- [59] A. Boyarsky, J. Lesgourgues, O. Ruchayskiy, and M. Viel, “Lyman-alpha constraints on warm and on warm-plus-cold dark matter models”, *JCAP* **0905** (2009) 012, [arXiv:0812.0010 \[astro-ph\]](#).
- [60] M. Kaplinghat, “Dark matter from early decays”, *Phys.Rev.* **D72** (2005) 063510, [arXiv:astro-ph/0507300](#).
- [61] K. Jedamzik, M. Lemoine, and G. Moulhaka, “Gravitino, axino, Kaluza-Klein graviton warm and mixed dark matter and reionisation”, *JCAP* **0607** (2006) 010, [arXiv:astro-ph/0508141](#).
- [62] S. Hannestad, “Neutrino physics from precision cosmology”, *Prog. Part. Nucl. Phys.* **65** (2010) 185–208, [arXiv:1007.0658 \[hep-ph\]](#).
- [63] J. Hamann, S. Hannestad, J. Lesgourgues, C. Rampf, and Y. Y. Wong, “Cosmological parameters from large scale structure - geometric versus shape information”, *JCAP* **1007** (2010) 022, [arXiv:1003.3999 \[astro-ph.CO\]](#).
- [64] WMAP Collaboration, E. Komatsu *et al.*, “Five-Year Wilkinson Microwave Anisotropy Probe (WMAP) Observations: Cosmological Interpretation”, *Astrophys.J.Suppl.* **180** (2009) 330–376, [arXiv:0803.0547 \[astro-ph\]](#).

- [65] M. C. Gonzalez-Garcia, M. Maltoni, and J. Salvado, “Updated global fit to three neutrino mixing: status of the hints of  $\theta_{13} > 0$ ”, *JHEP* **04** (2010) 056, [arXiv:1001.4524 \[hep-ph\]](#).
- [66] K. Abazajian, E. Calabrese, A. Cooray, F. De Bernardis, S. Dodelson, *et al.*, “Cosmological and Astrophysical Neutrino Mass Measurements”, *Astropart.Phys.* **35** (2011) 177–184, [arXiv:1103.5083 \[astro-ph.CO\]](#).
- [67] S. Joudaki and M. Kaplinghat, “Dark Energy and Neutrino Masses from Future Measurements of the Expansion History and Growth of Structure”, *Phys.Rev.* **D86** (2012) 023526, [arXiv:1106.0299 \[astro-ph.CO\]](#).
- [68] KATRIN Collaboration, A. Osipowicz *et al.*, “KATRIN: A Next generation tritium beta decay experiment with sub-eV sensitivity for the electron neutrino mass. Letter of intent”, [arXiv:hep-ex/0109033](#).
- [69] IGEX Collaboration, C. Aalseth *et al.*, “The IGEX Ge-76 neutrinoless double beta decay experiment: Prospects for next generation experiments”, *Phys.Rev.* **D65** (2002) 092007, [arXiv:hep-ex/0202026 \[hep-ex\]](#).
- [70] NEMO Collaboration, R. Arnold *et al.*, “First results of the search of neutrinoless double beta decay with the NEMO 3 detector”, *Phys.Rev.Lett.* **95** (2005) 182302, [arXiv:hep-ex/0507083](#).
- [71] K. Jedamzik, “Big bang nucleosynthesis constraints on hadronically and electromagnetically decaying relic neutral particles”, *Phys. Rev.* **D74** (2006) 103509, [arXiv:hep-ph/0604251](#).
- [72] W. Hu and J. Silk, “Thermalization constraints and spectral distortions for massive unstable relic particles”, *Phys.Rev.Lett.* **70** (1993) 2661–2664.
- [73] J. Chluba and R. Sunyaev, “The evolution of CMB spectral distortions in the early Universe”, [arXiv:1109.6552 \[astro-ph.CO\]](#).
- [74] J. C. Mather, E. Cheng, D. Cottingham, R. Eplee, D. Fixsen, *et al.*, “Measurement of the Cosmic Microwave Background spectrum by the COBE FIRAS instrument”, *Astrophys.J.* **420** (1994) 439–444.
- [75] D. Fixsen, E. Cheng, J. Gales, J. C. Mather, R. Shafer, *et al.*, “The Cosmic Microwave Background spectrum from the full COBE FIRAS data set”, *Astrophys.J.* **473** (1996) 576, [arXiv:astro-ph/9605054](#).
- [76] A. Kogut, D. Fixsen, D. Chuss, J. Dotson, E. Dwek, *et al.*, “The Primordial Inflation Explorer (PIXIE): A Nulling Polarimeter for Cosmic Microwave Background Observations”, *JCAP* **1107** (2011) 025, [arXiv:1105.2044 \[astro-ph.CO\]](#).

- [77] R. Khatri and R. A. Sunyaev, “Beyond  $\gamma$  and  $\mu$ : the shape of the CMB spectral distortions in the intermediate epoch,  $1.5 \times 10^4 < z < 2 \times 10^5$ ”, *JCAP* **1209** (2012) 016, [arXiv:1207.6654 \[astro-ph.CO\]](#).
- [78] T. R. Slatyer, “Energy Injection And Absorption In The Cosmic Dark Ages”, [arXiv:1211.0283 \[astro-ph.CO\]](#).
- [79] L. Covi, J. Hasenkamp, S. Pokorski, and J. Roberts, “Gravitino Dark Matter and general neutralino NLSP”, *JHEP* **11** (2009) 003, [arXiv:0908.3399 \[hep-ph\]](#).
- [80] T. Kanzaki, M. Kawasaki, K. Kohri, and T. Moroi, “Cosmological Constraints on Gravitino LSP Scenario with Sneutrino NLSP”, *Phys. Rev.* **D75** (2007) 025011, [arXiv:hep-ph/0609246](#).
- [81] E. J. Chun, D. Comelli, and D. H. Lyth, “The Abundance of relativistic axions in a flaton model of Peccei-Quinn symmetry”, *Phys.Rev.* **D62** (2000) 095013, [arXiv:hep-ph/0008133](#).
- [82] J. A. Cembranos, J. L. Feng, A. Rajaraman, and F. Takayama, “SuperWIMP solutions to small scale structure problems”, *Phys.Rev.Lett.* **95** (2005) 181301, [arXiv:hep-ph/0507150](#).
- [83] P. Colín, V. Avila-Reese, and O. Valenzuela, “Substructure and halo density profiles in a Warm Dark Matter Cosmology”, *Astrophys. J.* **542** (2000) 622–630, [arXiv:astro-ph/0004115](#).
- [84] E. Polisensky and M. Ricotti, “Constraints on the Dark Matter Particle Mass from the Number of Milky Way Satellites”, *Phys.Rev.* **D83** (2011) 043506, [arXiv:1004.1459 \[astro-ph.CO\]](#).
- [85] F. Borzumati, T. Bringmann, and P. Ullio, “Dark matter from late decays and the small-scale structure problems”, *Phys. Rev.* **D77** (2008) 063514, [arXiv:hep-ph/0701007](#).